

CONSTRAINTS ON THE BINARY PROPERTIES OF MID TO LATE T DWARFS FROM HUBBLE SPACE TELESCOPE WFC3 OBSERVATIONS

M. ABERASTURI¹, A.J. BURGASSER², A. MORA³, E. SOLANO¹, E. L. MARTÍN⁴, I. N. REID⁵ AND D. LOOPER⁶

¹Centro de Astrobiología (INTA-CSIC), Departamento de Astrofísica, PO Box 78, 28691 Villanueva de la Cañada, Madrid, Spain

²Center for Astrophysics and Space Science, University of California San Diego, La Jolla, CA, 92093, USA

³ESA–ESAC, Gaia SOC. P. O. Box 78 E-28691 Villanueva de la Cañada, Madrid, Spain

⁴Centro de Astrobiología (INTA-CSIC), Departamento de Astrofísica. Carretera de Ajalvir km 4, E-28550 Torrejón de Ardoz, Madrid, Spain

⁵Space Telescope Science Institute, 3700 San Martin Drive, Baltimore, MD 21218, USA and

⁶Institute for Astronomy, University of Hawaii, 2680 Woodlawn Drive, Honolulu, HI 96822

Draft version September 19, 2014

ABSTRACT

We used HST/WFC3 observations of a sample of 26 nearby (≤ 20 pc) mid to late T dwarfs to search for cooler companions and measure the multiplicity statistics of brown dwarfs. Tightly-separated companions were searched for using a double-PSF fitting algorithm. We also compared our detection limits based on simulations to other prior T5+ brown dwarf binary programs. No new wide or tight companions were identified, which is consistent with the number of known T5+ binary systems and the resolution limits of WFC3. We use our results to add new constraints to the binary fraction of T-type brown dwarfs. Modeling selection effects and adopting previously derived separation and mass ratio distributions, we find an upper limit total binary fraction of $<16\%$ and $<25\%$ assuming power law and flat mass ratio distributions respectively, which are consistent with previous results. We also characterize a handful of targets around the L/T transition.

Keywords: Brown dwarfs – stars: low-mass – binaries: general – Methods: observational – Techniques: photometric

1. INTRODUCTION

Since their first theoretical prediction (Kumar 1963; Hayashi & Nakano 1963), brown dwarfs (BDs), objects with insufficient mass to sustain stable hydrogen fusion, have bridged the gap in temperature and mass between cold, very low mass stars (VLM; $M_{\odot} \geq 0.075 M_{\odot}$) and the hottest, most massive giant planets ($M_{\odot} \leq 0.013 M_{\odot}$; Chabrier et al. 2000; Burrows et al. 2003). Since the first discoveries of brown dwarfs as companions to low luminosity sources, GD165B (Becklin & Zuckerman 1988) and Gl229B (Nakajima et al. 1995; Golimowski et al. 1995; Oppenheimer et al. 1995) and free-floating systems (Rebolo et al. 1995; Ruiz et al. 1997; Martin et al. 1997), three new spectral classes have been introduced to characterize these low mass objects: L dwarfs ($T_{\text{eff}} \sim 2500$ K – 1500K, Kirkpatrick et al. 1999, Martín et al. 1999), T dwarfs ($T_{\text{eff}} \sim 1500$ K – 500K, Burgasser et al. 2006a) and Y dwarfs ($T_{\text{eff}} \leq 500$ K; Cushing et al. 2011). With photospheres dominated by condensate clouds in L dwarfs and molecular gas species in T and Y dwarfs, BDs allow us to study planetary-like atmospheres without having to eliminate the glare of a host star. Thanks to wide-field infrared and optical imaging surveys such as the Two Micron All Sky Survey (2MASS, Skrutskie et al. 2006) and DEep Near Infrared Survey of the southern sky (DENIS, Epchtein et al. 1997) and spectroscopic surveys as Sloan Digital Sky Survey (SDSS, York et al. 2000), we now know of

~ 1000 L and T type BDs belonging to the field and young stellar clusters¹. More recently, deeper near and mid-infrared surveys like the UKIRT Infrared Deep Sky Survey (UKIDSS, Lawrence et al. 2007), the Canada-France Brown Dwarf Survey (CFBDS, Delorme et al. 2008) and the Wide-field Infrared Survey Explorer (WISE; Wright et al. 2010), have allowed us to explore the regime of late T and Y dwarfs. Most Y dwarfs have been identified as isolated field objects in WISE (e.g., Kirkpatrick et al. 2011; Tinney et al. 2012), but discoveries such as WD 0806-661B (Luhman et al. 2011) and CFBDSIR J1458+1013B (Liu et al. 2011), demonstrate the continued utility of companion searches.

Beyond discovery, searches for companions allow us to measure the statistics of multiple systems, which are particularly useful for testing formation scenarios for VLM stars and BDs. While the binary fraction (BF) of solar-type stellar systems is $\sim 65\%$ (Duquennoy & Mayor 1991) and early-type M stars $\sim 30\%$ – 40% (Reid & Gizis 1997b; Delfosse et al. 2004), measurement of multiplicity statistics for BDs have inferred fractions of 15% – 30% (Allen 2007; Burgasser 2007), indicating a mass dependence either in multiple formation or in the subsequent evolution of multiple systems.

The majority of the ~ 100 VLM binary systems now known were uncovered with high angular resolution Hubble Space Telescope (HST) and/or ground-based adaptive optics (AO) imaging programs (Liu et al. 2006;

Based on observations made with the NASA/ESA Hubble Space Telescope, obtained at the Space Telescope Science Institute, which is operated by the Association of Universities for Research in Astronomy Inc., under NASA contract NAS 5-26555. These observations are associated with programs 11631 and 11666.

¹ See <http://dwarfarchives.org> for an up-to-date list of L, T and Y dwarfs.

Siegler et al. 2007). Those studies find that BD systems peak in mass ratio at $M_2/M_1 \approx 0.8$ with separations typically closer than $a < 20$ AU (Allen 2007). The statistics of VLM binaries have motivated new theories of BD formation, via turbulent fragmentation (Bate 2009) or gravitational instability in circumstellar disks (Stamatellos & Whitworth 2009). Other techniques such as astrometry and analysis of microlensing events are reaching the sensitivity required to detect BD binaries with low mass ratios, and even giant planets around BDs (Burgasser et al. 2010, Rodler et al. 2011; Sahlmann et al. 2013; Choi et al. 2013). Additionally, other techniques such as astrometry, high precision radial velocities, microlensing and blended-light spectroscopy are reaching the sensitivity required to detect BD binaries with low mass ratios, and even giant planets around BDs (Burgasser et al. 2010, Rodler et al. 2011; Sahlmann et al. 2013; Choi et al. 2013).

These studies can be advanced by increasing the population of known brown dwarf binary systems. To do this, we undertook two parallel programs using the Wide Field Camera 3 (WFC3) installed on the Hubble Space Telescope. Observations, sample composition and data reduction are described in Section 2. In Section 3 we present the photometric results and define new color/spectral type relations. In Section 4 we describe the results of point-spread function (PSF) fits to our sample and results. We also quantify the WFC3 detection limits which prove to be the limitation in our study. In section 5, we infer a bias corrected BD binary fraction through simulation, and compare these results with previous surveys. Finally, in Section 6 we summarize the main results of our project.

2. OBSERVATIONS

2.1. Sample

Our original sample consists of 37 nearby sources ($d \leq 30$ pc) identified as L or T dwarfs based on prior searches of 2MASS, DENIS, SDSS or UKIDSS. Measurements of the infrared photometry (2MASS and MKO systems), proper motions (PMs) and distances for the whole sample are listed in Table 1. We have used the Dupuy & Liu (2012a) absolute magnitude–SpT relation to estimate the photometric distances for six objects without parallax measurement. The sources were observed as part of two HST(WFC3) programs (11631 and 11666) with slightly different goals:

- Program 11631 targeted 11 L and early T dwarfs, including one known resolved binary 2MASS J1520–4422AB (Burgasser et al. 2007) and one previously unreported L3 source, DENIS J1013–7842 (Looper et al in prep). We present additional information of these sources in Appendix A and B, respectively. The 11631 program aimed to explore multiplicity across the L/T transition and was used here to estimate magnitude-color and color-near infrared spectral type (NIR SpT) relations. The observations were obtained between January 2010 and June 2011.
- Program 11666 targeted 26 mid and late-T dwarfs (from T5 to T8.5) to search Y dwarf companions,

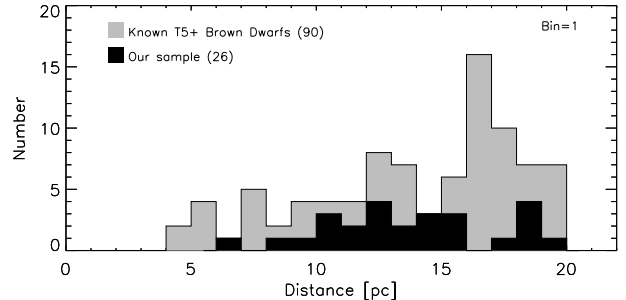


Figure 1. Number of known brown dwarfs with SpT \geq T5 from Brown Dwarf Archive, Gelino et al. 2011, Mužić et al. 2012, Bihain et al. 2013, Beichman et al. 2013 and Cushing et al. 2014. The photometric distances were determined using the Dupuy & Liu (2012a) absolute magnitude–SpT relation.

with measured or estimated distances ≤ 20 pc not previously observed by HST or ground-based AO programs, with the exception of two sources with insufficient data (SDSS J1346–0031 and 2MASS J0727+1710). The observations were obtained between November 2009 and October 2010. The sample includes two of the coolest objects known at that time: ULAS J0034-0052 (Warren et al. 2007) and ULAS J1238+0953 (Bunningham et al. 2008). We included one previously unreported T6 dwarf, 2MASS J2237+7228 (see more details in Appendix C). In Fig.1 we compare our sample against the number of known T5+ dwarfs within 20 parsecs; our sample includes $\sim 29\%$ of such systems. We consider this sample statistically representative to estimate the binary fraction (BF) for the mid-late T dwarfs.

The programs were originally planned for Near Infrared Camera and Multi-Object Spectrometer (NICMOS/NIC1) given that instrument’s demonstrated ability to identify cold BD companions (Burgasser et al. 2006b, Stumpf et al. 2011), but an instrument failure forced the change to WFC3.

2.2. Imaging and Data Reduction

The IR channel of WFC3 was used in both programs. The detector (HgCdTe) is a 1024x1024 pixel array with an angular resolution of $0.13''/\text{pixel}$ and a field of view of $123'' \times 136''$. The camera has 16 filters covering wide (W), medium (M) and narrow (N) bands from 800 to 1700nm. The observations analysed here use the F110W, F127M, F139M and F164N filters (see Fig. 2). F110W ($\lambda_c \equiv 1.1191 \mu\text{m}$) is the widest filter covering Y and J bands, encompassing the peak emission of flux from L and T dwarfs in the near infrared. F127M ($\lambda_c \equiv 1.274 \mu\text{m}$) covers the $1.27 \mu\text{m}$ peak in late-T dwarfs. Finally F139M ($\lambda_c \equiv 1.3838 \mu\text{m}$) and F164N ($\lambda_c \equiv 1.6460 \mu\text{m}$) cover H_2O and CH_4 absorption bands in L and T dwarfs, respectively. Program 11631 (L and early T dwarfs) utilised the F127M, F139M and F164N filters; Program 11666 (mid-late T dwarfs) data were taken using the F110W, F127M and F164N filters.

Images were taken in MULTIACCUM mode following a standard dither pattern (4 dithers). Exposure times ranged from 111.0s for the widest filter to 1197.7s

Table 1
L and T dwarfs sample

Name	NIR–SpT Literature	α (J 2000) hh:mm:ss	δ (J 2000) hh:mm:ss	J (mag)	H (mag)	K_s (mag)	$\mu_{\alpha\cos\delta}$ (mas yr^{-1})	μ_{δ} (mas yr^{-1})	Distance (pc)
(1)	(2)	(3)	(4)	(5)	(6)	(7)	(8)	(9)	(10)
Program 11631									
Name	NIR–SpT Literature	α (J 2000) hh:mm:ss	δ (J 2000) hh:mm:ss	J (mag)	H (mag)	K_s (mag)	$\mu_{\alpha\cos\delta}$ (mas yr^{-1})	μ_{δ} (mas yr^{-1})	Distance (pc)
(1)	(2)	(3)	(4)	(5)	(6)	(7)	(8)	(9)	(10)
2MASS J0340-6724	L7:: ^a	03:40:09.42	-67:24:05.1	14.74 \pm 0.03	13.59 \pm 0.03	12.93 \pm 0.03	-318.0 \pm 7.0	508.0 \pm 18.0	11.0 \pm 3.0
SDSS J0739+6615	T1.5+/-1	07:39:22.26	+66:15:03.9	16.82 \pm 0.13	16.00 \pm 0.10	15.83 \pm 0.18	180.0 \pm 10.0	-77.0 \pm 26.0	34.0 \pm 4.0
DENIS J1013-7842	L3 ^a	10:13:25.88	-78:42:55.3	13.84 \pm 0.03	12.74 \pm 0.03	12.03 \pm 0.03	14.2 \pm 1.3
2MASS J1122-3512	T2	11:22:08.26	-35:12:36.3	15.02 \pm 0.04	14.36 \pm 0.05	14.38 \pm 0.07	-150.0 \pm 40.0	-250.0 \pm 30.0	15.0 \pm 1.0
SDSS J1439+3042	T2.5	14:39:45.95	+30:42:21.0	17.22 \pm 0.23	>16.28	>15.88	29.9 \pm 7.5
SDSS J1511+0607	T2	15:11:14.66	+06:07:43.1	15.88 \pm 0.02	15.14 \pm 0.02	14.52 \pm 0.10	-255.6 \pm 7.1	-238.0 \pm 7.0	18.0 \pm 3.0
2MASS J1520-4422A	L1.5	15:20:02.30	-44:22:41.9	13.22 \pm 0.03	12.36 \pm 0.03	11.89 \pm 0.03	-630.0 \pm 30.0	-370.0 \pm 20.0	19.0 \pm 1.0
2MASS J1520-4422B	L4.5	15:20:02.30	-44:22:41.9	14.70 \pm 0.07	13.70 \pm 0.05	13.70 \pm 0.05	-630.0 \pm 30.0	-370.0 \pm 20.0	19.0 \pm 1.0
Program 11666									
ULAS J0034-0052 ^b	T8.5	00:34:02.76	-00:52:08.0	18.15 \pm 0.08	18.49 \pm 0.04	18.48 \pm 0.05	12.6 \pm 0.6
HD3651B ^b	T7.5	00:39:18.61	+21:15:12.7	16.16 \pm 0.03	16.68 \pm 0.04	16.87 \pm 0.0	-461.1 \pm 0.7	-370.9 \pm 0.7	11.0 \pm 0.3
2MASS J0050-3322	T7	00:50:19.92	-33:22:41.4	15.93 \pm 0.07	15.84 \pm 0.19	15.24 \pm 0.19	1200.0 \pm 110.0	900.0 \pm 120.0	8.0 \pm 1.0
SDSS J0325+0425	T5.5	03:25:53.11	+04:25:40.0	16.25 \pm 0.14	>16.08	16.37 \pm 0.06	-163.7 \pm 5.8	-59.6 \pm 5.7	19.0 \pm 2.0
2MASS J0407+1514	T5	04:07:08.94	+15:14:55.4	16.06 \pm 0.09	16.02 \pm 0.21	15.92 \pm 0.26	106.0 \pm 16.0	-110.0 \pm 17.0	17.0 \pm 2.0
2MASS J0510-4208	T5	05:10:35.32	-42:08:08.2	16.22 \pm 0.09	16.24 \pm 0.16	16.0 \pm 0.28	104.0 \pm 15.0	580.0 \pm 21.0	18.0 \pm 2.0
2MASS J0727+1710	T7	07:27:19.07	+17:09:52.2	15.60 \pm 0.06	15.76 \pm 0.17	15.55 \pm 0.19	1046.0 \pm 4.0	-767.0 \pm 3.0	9.1 \pm 0.2
2MASS J0729-3954	T8pec	07:28:59.47	-39:53:46.3	15.92 \pm 0.08	15.98 \pm 0.18	>15.29	-566.6 \pm 5.3	1643.4 \pm 5.5	6.0 \pm 1.0
2MASS J0741+2351	T5	07:41:48.96	+23:51:25.9	16.15 \pm 0.10	15.84 \pm 0.18	>15.85	-243.0 \pm 13.0	-143.0 \pm 14.0	18.0 \pm 2.0
2MASS J0939-2448	T8	09:39:35.87	-24:48:38.0	15.98 \pm 0.11	15.80 \pm 0.15	>16.56	558.1 \pm 5.8	-1030.5 \pm 5.6	10.0 \pm 2.0
2MASS J1007-4555	T5	10:07:32.99	-45:55:13.3	15.65 \pm 0.07	15.68 \pm 0.12	15.56 \pm 0.23	-723.5 \pm 3.4	148.7 \pm 3.6	15.0 \pm 2.0
2MASS J1114-2618	T7.5	11:14:48.90	-26:18:27.2	15.86 \pm 0.08	15.73 \pm 0.12	>16.11	-2927.2 \pm 7.0	-374.2 \pm 7.2	10.0 \pm 2.0
2MASS J1231+0847	T5.5	12:31:46.74	+08:47:22.3	15.57 \pm 0.07	15.31 \pm 0.11	15.22 \pm 0.19	-1176.0 \pm 21.0	-1043.0 \pm 21.0	12.0 \pm 1.0
ULAS J1238+0953 ^b	T8.5	12:38:28.57	+09:53:51.3	18.95 \pm 0.02	19.20 \pm 0.02	18.5 \pm 4.3
SDSS J1250+3925	T4	12:50:11.67	+39:25:47.9	16.54 \pm 0.11	16.18 \pm 0.18	15.05 \pm 0.24	-15.0 \pm 8.0	-828.0 \pm 11.0	23.0 \pm 2.0
SDSS J13464-0031	T6.5	13:46:46.04	-00:31:51.3	16.00 \pm 0.10	15.46 \pm 0.12	15.77 \pm 0.27	-503.0 \pm 3.0	-114.0 \pm 2.0	14.6 \pm 0.3
SDSS J1504+1027	T7	15:04:11.74	+10:27:16.8	17.03 \pm 0.23	>16.90	>17.02	373.8 \pm 7.9	-322.5 \pm 7.7	15.9 \pm 2.5
SDSS J1628+2308	T7	16:28:38.99	+23:08:18.4	16.45 \pm 0.10	16.11 \pm 0.15	15.87 \pm 0.24	497.0 \pm 20.0	-461.0 \pm 21.0	14.0 \pm 4.0
2MASS J1754+1649	T5	17:54:54.56	+16:49:18.1	15.81 \pm 0.07	15.65 \pm 0.13	15.55 \pm 0.16	113.5 \pm 9.1	-141.4 \pm 9.2	14.3 \pm 1.3
SDSS J1758+4633	T6.5	17:58:05.49	+46:33:17.1	16.15 \pm 0.08	16.25 \pm 0.21	15.46 \pm 0.19	26.0 \pm 15.0	594.0 \pm 16.0	12.0 \pm 2.0
2MASS J1828-4849	T5.5	18:28:36.01	-48:49:02.6	15.18 \pm 0.06	14.91 \pm 0.07	15.18 \pm 0.14	231.4 \pm 10.5	52.4 \pm 10.9	11.0 \pm 1.0
2MASS J1901+4718	T5	19:01:05.89	+47:18:09.9	15.86 \pm 0.07	15.47 \pm 0.09	15.64 \pm 0.29	-110.0 \pm 20.0	-360.0 \pm 20.0	15.0 \pm 2.0
SDSS J2124+0100	T5	21:24:14.02	+01:00:02.7	16.03 \pm 0.07	16.18 \pm 0.20	>16.14	202.0 \pm 14.0	287.0 \pm 14.0	18.0 \pm 2.0
2MASS J2154+5942	T5	21:54:32.98	+59:42:14.4	15.66 \pm 0.07	15.76 \pm 0.17	>15.34	-182.0 \pm 9.0	-445.0 \pm 17.0	10.0 \pm 1.0
2MASS J2237+7228	T6 ^a	22:37:20.47	+72:28:35.3	15.76 \pm 0.07	15.94 \pm 0.21	>15.99	-73.0 \pm 2.0	-116.0 \pm 2.0	13.0 \pm 2.0
2MASS J2331-4718	T5	23:31:23.84	-47:18:28.2	15.66 \pm 0.07	15.51 \pm 0.15	15.39 \pm 0.2	104.0 \pm 13.0	-49.0 \pm 19.0	13.0 \pm 2.0
2MASS J2359-7335	T6.5	23:59:41.09	-73:35:04.9	16.17 \pm 0.04	16.06 \pm 0.07	16.05 \pm 0.13	12.3 \pm 1.9

Note. — (1) Cruz et al. (2007); (2) Chiu et al. (2006); (3) Tinney et al. (2005); (4) Burgasser et al. (2007); (5) Warren et al. (2007); (6) Mugrauer et al. (2000); (7) Looper et al. (2007); (8) Burgasser et al. (2002); (9) Knapp et al. (2004); (10) Burningham et al. (2008); (11) Tsvetanov et al. (2000); (12) Faherty et al. (2011); (13) Faherty et al. (2009); (14) Warren et al. (2007); (15) Luhman et al. (2007); (16) Luhman et al. (2007); (17) Luhman et al. (2007); (18) Vrba et al. (2004); (19) Tinney et al. (2003); (20) Kendall et al. (2007b); (21) Dupuy & Liu (2012a); (22) Dupuy & Liu (2012a); (23) Albert et al. (2011).

^a Optical spectral type.

^b *MKO* photometry.

^c Distance estimated from the Dupuy & Liu (2012a) absolute magnitude–SpT relation.

for the narrowest (Table 2). Due to read time limits the images in F110W, F127M and F139M filter (in program 11631) cover an area of 35.88'' x 31.98'' (276 x 246 pixels), while the images in F164N filter and F127M (in program 11666) cover 141.70'' x 125.32'' (1090 x 964 pixels). We used the pipeline processed images, which include the analog-to-digital correction, subtraction of bias and dark current, linearity correction for readout artifacts, flat-field image and photometric calibration. The corrected images were used as input in MultiDrizzle (Fruchter & Hook 2002) to perform the geometric distortion correction on all individual images, cosmic-ray rejection, and the final combination of the dithered images into a single output final image.

Upon visual inspection of the images, we rejected three objects from our original sample. 2MASS J094908.6–154548.5 (Tinney et al. 2005) was rejected due to poor image quality. Due to its high proper motion, 2MASS J11263991-5003550 (Folkes et al. 2007) was located outside the field of view at the time at observations. SIMP J132407.76+190627.1 (Deacon et al. 2011) was missed due to erroneous telescope pointing. Our final sample consists of 34 sources.

3. WFC3 PHOTOMETRY

3.1. Measurements

We used SExtractor (Bertin & Arnouts 1996) to measure the photometry for different aperture sizes around sources in our final calibrated images. We used aper-

Table 2
Log of observations. Magnitude limits for $\rho=0.6''$

Name	F110W			F127M			F139M			F164N			Observation UT Date
	t ^a (s)	Δm_{lim}^b (mag)	m_{lim}^c (mag)	t (s)	Δm_{lim}^b (mag)	m_{lim}^c (mag)	t (s)	Δm_{lim}^b (mag)	m_{lim}^c (mag)	t (s)	Δm_{lim}^b (mag)	m_{lim}^c (mag)	
(1)	(2)	(3)	(4)	(5)	(6)	(7)	(8)	(9)	(10)	(11)	(12)	(13)	(14)
Program 11631													
2MASS J0340-6724	413	2.5	17.25	413	2.0	17.45	413	2.0	15.60	2011-08-06
SDSS J0739+6615	413	2.0	18.61	413	1.5	19.82	413	2.0	18.03	2011-06-03
2MASS J1013-7842	413	2.0	16.19	413	2.25	16.53	413	1.75	14.49	2011-07-23
2MASS J1122-3512	413	1.75	16.45	413	1.75	18.30	413	1.75	16.01	2011-08-13
SDSS J1439+3042	413	2.0	18.78	413	1.75	20.25	413	2.0	18.50	2011-07-16
SDSS J1511+0607	413	2.0	17.60	413	2.0	18.68	413	2.0	17.11	2011-05-08
2MASS J1520-4422A	413	2.25	16.14	413	2.0	16.10	413	1.5	14.23	2011-07-01
Program 11666													
ULAS J0034-0052	111.0	2.0	21.46	997	2.0	19.71	1198	1.75	21.36	2010-12-27
HD3651B	133.0	2.5	19.94	997	1.75	17.60	1198	2.5	21.21	2010-12-30
2MASS J0050-3322	155.1	2.25	19.17	997	2.25	17.87	1198	2.25	18.89	2011-06-08
SDSS J03255+0425	111.0	2.75	19.92	997	2.0	17.78	1198	2.25	18.75	2010-12-02
2MASS J04070+1514	111.0	1.75	18.45	997	3.0	18.72	1198	2.25	18.41	2011-03-24
2MASS J0510-4208	67	2.0	19.12	997	2.25	18.00	1348	2.5	18.74	2011-04-03
2MASSI J0727+1710	133	1.75	18.13	997	2.75	17.93	1198	2.5	18.87	2010-11-11
2MASS J0729-3954	177	2.0	19.00	997	3.0	18.46	1198	2.0	18.64	2011-05-29
2MASS J07414+2351	133	2.0	18.92	997	2.25	18.23	1198	1.75	18.29	2010-11-09
2MASS J0939-2448	133	2.25	19.17	997	2.0	17.64	1198	2.0	18.92	2010-12-12
2MASS J1007-4555	111	2.25	18.64	997	2.25	17.85	1198	1.5	17.57	2011-05-14
2MASS J1114-2618	133.	2.0	18.62	997	2.25	17.87	1198	1.5	18.19	2010-12-08
2MASS J1231+0847	111	2.25	18.72	997	2.0	17.22	1198	3.0	18.72	2011-07-15
ULAS J1238+0953	111	2.25	21.88	997	1.75	19.98	1198	1.25	21.56	2011-02-23
SDSS J1250+3925	177	2.5	19.91	997	2.25	18.38	1198	2.25	18.41	2011-06-08
SDSSP J1346-0031	111	1.75	18.91	997	3.0	18.48	1198	2.0	18.46	2011-07-17
SDSS J1504+1027	111	1.5	18.87	997	2.0	18.12	1198	1.5	18.88	2011-06-24
SDSS J1628+2308	133	2.0	19.29	997	2.5	18.44	1198	1.25	18.49	2011-02-10
2MASS J1754+1649	133	2.5	18.91	997	2.0	17.53	1198	1.75	17.55	2011-07-19
SDSS J1758+4633	111	1.75	18.65	997	2.0	17.70	1348	1.75	18.35	2010-12-09
2MASS J1828-4849	111	1.75	17.95	997	1.75	16.79	1348	1.75	17.00	2011-10-23
2MASS J1901+4718	111	2.0	18.45	997	2.25	17.67	1348	1.5	17.20	2010-12-14
SDSS J21241+0100	111	2.5	19.41	997	2.25	17.97	1198	2.0	18.19	2010-11-21
2MASS J2154+5942	177	2.0	18.38	997	2.75	18.24	1198	1.75	17.873	2010-12-01
2MASS J2237+7228	177	1.5	17.90	1197	2.5	18.10	1348	1.5	17.41	2011-05-18
2MASS J2331-4718	111	2.25	18.50	997	2.25	17.58	1348	2.0	17.53	2011-04-13
2MASS J2359-7335	177	2.5	19.62	1197	2.25	18.24	1348	1.75	18.77	2010-11-02

^aExposure time.

^bLimit Δm measured from Monte Carlo simulations for each object (see Section 4.3).

^cLimiting magnitude calculated from Monte Carlo simulations and their respective magnitudes for each object.

ture diameters from 2 to 19 pixels ($0.26''$ - $2.6''$) around each source, and a common background annulus of 25 pixels ($3.25''$). The integrated counts were transformed to Vega magnitudes with the corresponding conversion factors provided in the WFC3 instruments manual.

In order to estimate the aperture correction for our sample we chose three isolated sources common in F110W, F127M and F164N, SDSSJ0325+0425, 2MASSJ1231+0847 and SDSSJ1346-0031. We used 2MASS J0340-6724, SDSS J0739+6615 and SDSS J1511+0607 for the F139M filter. Comparison of integrated flux profiles as a function of aperture size normalized to a 20-pixel aperture demonstrates excellent agreement between the sources, with deviations of less than 0.009 mag for apertures wider than 10 pixels (see Table 3). We adopted, a 6 pixel aperture diameter ($0.78''$) to extract the photometry. To calculate the total uncertainties in the magnitude corrections, we combined count uncertainties, a 1% error due to instrumental photometric stability, and 1% due to flux calibration uncertainty (see WFC3 manual²). Final values are listed in Table 4.

Table 3
WFC3 Aperture Corrections.

Radius (pixels)	F110W (mag)	F127M (mag)	F39M (mag)	F164N (mag)
2	-1.38±0.08	-1.26±0.1	-1.08±0.05	-1.30 ±0.07
3	-0.77±0.06	-0.62±0.06	-0.59±0.05	-0.72±0.04
4	-0.42±0.05	-0.36±0.04	-0.32±0.02	-0.43±0.03
5	-0.27±0.03	-0.23±0.03	-0.21±0.01	-0.28±0.01
6	-0.20±0.03	-0.17±0.02	-0.16±0.007	-0.20±0.01
7	-0.17 ±0.02	-0.15±0.02	-0.13±0.005	-0.15±0.007
8	-0.14±0.02	-0.12±0.01	-0.12±0.004	-0.13±0.006
9	-0.11 ±0.01	-0.10±0.01	-0.10±0.003	-0.11±0.004
10	-0.09±0.01	-0.08±0.009	-0.08±0.003	-0.09±0.003
11	-0.08 ±0.01	-0.07±0.008	-0.06±0.002	-0.08±0.0002
12	-0.07±0.009	-0.06±0.007	-0.05±0.002	-0.06±0.001
13	-0.06±0.007	-0.05±0.006	-0.04±0.003	-0.05±0.001
14	-0.05±0.006	-0.04±0.004	-0.04±0.003	-0.04±0.001
15	-0.04±0.005	-0.03±0.003	-0.03±0.003	-0.03±0.001
16	-0.03±0.003	-0.02±0.002	-0.02±0.001	-0.03±0.001
17	-0.02±0.002	-0.02±0.002	-0.01±0.001	-0.02±0.0007
18	-0.012±0.001	-0.01±0.001	-0.01±0.002	-0.01±0.0009
19	-0.006±0.0006	-0.005±0.0006	-0.006±0.001	-0.006±0.0004

3.2. *L* and *T* dwarf colors

To provide adequate color discrimination of L and T dwarfs from background sources, we examined all possible color combinations. While the majority of back-

² <http://www.stsci.edu/hst/wfc3>

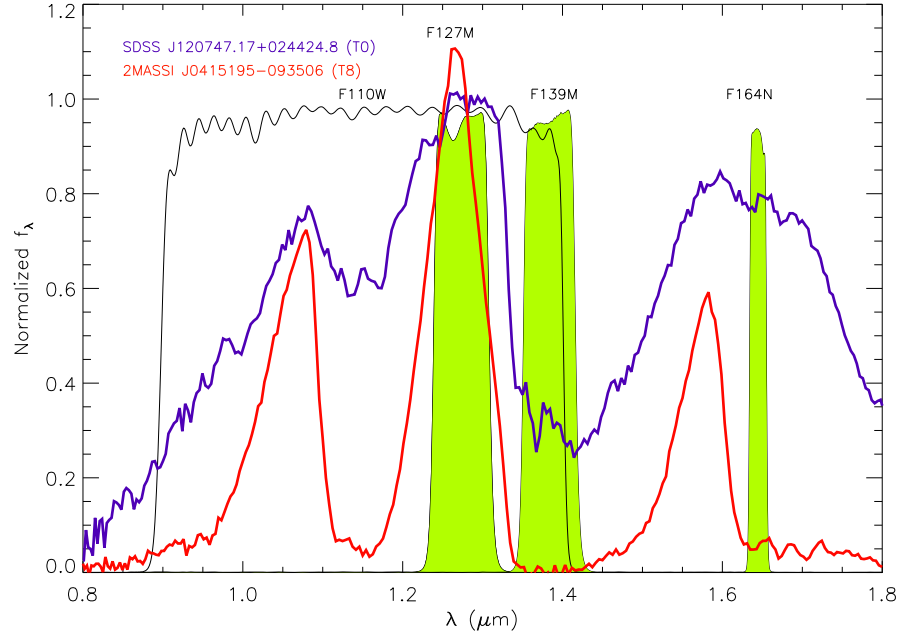


Figure 2. Filter transmission profiles of F110W (black line), F127M, F139M and F164N (green areas), compared to the near infrared spectra of the T8 2MASS J0415-0935 (Burgasser et al. 2004) and the T0 SDSS J1207+0244 (Looper et al. 2007)

Table 4
WF3 Photometry for 11631 and 11666 programs.

Name	NIR-SpT	F110W	F127M	F139M	F164N	F127M - F164N
(1)	Literature	(mag)	(mag)	(mag)	(mag)	(mag)
(2)	(3)	(4)	(5)	(6)	(7)	
Program 11631						
2MASS J0340-6724	L7.:	...	14.76±0.02	15.45±0.01	13.60±0.01	1.16±0.02
SDSS J0739+6615	T1.5+/-1	...	16.61±0.02	18.32±0.01	16.03±0.01	0.58±0.02
2MASS J1013-7842	L3	...	14.19±0.02	14.28±0.01	12.74±0.01	1.45±0.02
2MASS J1122-3512	T2	...	14.70±0.02	16.55±0.01	14.26±0.01	0.44±0.02
SDSS J1439+3042.	T2.5	...	16.78±0.02	18.50±0.01	16.50±0.01	0.28±0.02
SDSS J1511+0607.	T2	...	15.60±0.02	16.68±0.01	15.11±0.01	0.49±0.02
2MASS J1520-4422A	L1.5	...	13.89±0.02	14.10±0.01	12.73±0.01	1.16±0.02
2MASS J1520-4422B	L4.5	...	14.57±0.02	15.06±0.01	13.60±0.01	0.97±0.02
Program 11666						
ULAS J0034-0052	T8.5	19.46±0.03	17.71±0.02	...	19.61±0.02	-1.90±0.03
HD 3651B	T7.5	16.92±0.03	15.98±0.02	...	16.54±0.01	-1.85±0.02
2MASS J0050-3322	T7	16.92±0.03	15.62±0.02	...	16.64±0.01	-1.03±0.02
SDSS J0325+0425	T5.5	17.17±0.03	15.78±0.02	...	16.50±0.01	-0.72±0.02
2MASS J0407+1514	T5	16.70±0.03	15.72±0.02	...	16.16±0.01	-0.44±0.02
2MASS J0510-4208	T5	17.12±0.03	15.75±0.02	...	16.24±0.01	-0.49±0.02
2MASSI J0727+171	T7	16.38±0.03	15.18 ±0.02	...	16.37±0.01	-1.18±0.02
2MASS J0729-3954	T8pec	17.00±0.03	15.46±0.02	...	16.64±0.01	-1.18±0.02
2MASS J0741+2351	T5	16.92±0.03	15.98±0.02	...	16.54±0.01	-0.56±0.02
2MASS J0939-2448	T8	16.92±0.03	15.64±0.02	...	16.93±0.01	-1.28±0.02
2MASS J1007-4555	T5	16.39±0.03	15.60±0.02	...	16.07±0.01	-0.47±0.02
2MASS J1114-2618	T7.5	16.62± 0.03	15.62±0.02	...	16.69±0.01	-1.07±0.02
2MASS J1231+0847	T5.5	16.47± 0.03	15.22±0.02	...	15.73±0.01	-0.50±0.02
ULAS J1238+0953	T8.5	19.63±0.03	18.23±0.02	...	20.31±0.01	-2.08±0.04
SDSS J1250+3925	T4	17.42±0.03	16.13±0.02	...	16.16±0.01	-0.03±0.02
SDSSP J1346-0031	T6.5	17.16±0.03	15.48±0.02	...	16.46±0.01	-0.99±0.02
SDSS J1504+1027	T7	17.37± 0.03	16.13±0.02	...	17.38±0.01	-1.25±0.02
SDSS J1628+2308	T7	17.29±0.03	15.94±0.02	...	17.24±0.01	-1.29 ±0.02
2MASS J1754+1649	T5	16.41±0.03	15.53±0.02	...	15.80±0.01	-0.27±0.02
SDSS J1758+4633	T6.5	16.90±0.03	15.70±0.02	...	16.60±0.01	-0.89±0.02
2MASS J1828-4849	T5.5	16.20±0.03	15.04±0.02	...	15.24±0.01	-0.20±0.02
2MASS J1901+4718	T5	16.45 ±0.03	15.43±0.02	...	16.70±0.01	-0.27±0.02
SDSS J2124+0100	T5	16.91±0.03	15.72±0.02	...	16.19±0.01	-0.47±0.02
2MASS J2154+5942	T5	16.39 ±0.03	15.50±0.02	...	16.12±0.01	-0.63±0.02
2MASS J2237+7228	T6	16.40±0.03	15.60±0.02	...	15.91±0.01	-0.31±0.02
2MASS J2331-4718	T5	16.25±0.03	15.33±0.02	...	15.53±0.01	-0.19±0.02
2MASS J2359-7335	T6.5	17.12 ±0.03	16.00±0.02	...	17.02±0.01	-1.03±0.02

ground sources have neutral NIR colors, our targets show very red colors (see Table 4) due to molecular absorption. Figure 3 displays the magnitude vs. color and color vs. NIR-SpT³ of our targets. F110W–F164N shows considerable scatter vs. spectral type, so we did not calculate a spectral type relation for this color. This is likely due to the width at the F110W filter. F127M–F139M color displays a strong trend with spectral type in the late–L and early–T dwarfs. A linear fit to F127M–F139M color yields,

$$SpT = 1.56 - 6.25 * (F127M - F139M) \quad (1)$$

where SpT(L0) = 0, SpT(T5) = 15 and, SpT(Y0) = 20. The scatter is 1.2 subtypes.

Similarly, a quadratic fit of F127M–F164N color to SpT yields,

$$SpT = 13.22 - 5.37 * (F127M - F164N) - 1.56 * (F127M - F164N)^2 \quad (2)$$

The scatter in this relation is 0.6 subtypes and hence this color is a more accurate proxy for spectral type than F127M–F139M color.

Both trends reflect the strengthened H_2O and CH_4 absorption bands along the L and T sequence. Because these bands saturate, continuum fluxes also decline in the Y dwarf regime (Cushing et al. 2011; Kirkpatrick et al. 2011), so the trends may not persist to arbitrarily low temperatures.

4. WFC3/HST PSF FITTING ANALYSIS

4.1. Method

The main goal of this study is to identify binary systems in the sample. There are no well-resolved pairs other than the previously identified 2MASS J1520–4422AB (Burgasser et al. 2007; Kendall et al. 2007a). To identify more closely-separated pairs with blended PSFs, we used a PSF-fitting algorithm similar to that described in Burgasser et al. (2003).

In previous studies (Burgasser et al. 2006b; Dupuy & Liu 2012a), the Tiny Tim⁴ program (Krist 1995) has been used to generate a super-sampled PSF model that takes into account the source SED and instrument response. This tool does not currently implement oversampling for WFC3, so we decided to generate PSF models of each filter from the data. The WFC3 diffraction limit goes from 0.096'' for the bluest filter, F110W, to 0.142'' for the reddest one F164N. Therefore, we extracted subimages of 20x20 pixels (2.6''x 2.6'') centered on point sources, which were then resampled at ten times the original pixel size and recentered by subpixel offsets. We median-combined 83 background sources in F110W, 399 sources in F127M, 12 sources in F139M and 515 sources in F164N images to create the PSF models. We found these models provide superior fits to the target than the WFC3 TinyTim model.

³ Except for 2MASS J0340–6724, 2MASS J1013–7842 and 2MASS J2237+7228 where only the optical spectral type was available.

⁴ <http://tinytim.stsci.edu/cgi-bin/tinytimweb.cgi>

To search for faint companions, we used an iterative routine focused on the same 2.6''x 2.6'' subimages centered on each target. First, initial guesses for the positions and fluxes for two components were made using a simple peak detection on the original image (for the primary) and on the residual image after PSF subtraction (for the secondary). The routine then finds the optimal primary and secondary position by shifting in steps of 0.1 pixels and flux scaling in steps of 1% (0.01mag). The quality of fit was assessed using the χ^2 statistic:

$$\chi^2 = \sum_{ij} \frac{(D_{ij} - \alpha M_{ij})^2}{\sigma_{ij}^2} \quad (3)$$

Here D_{ij} is the data, M_{ij} is the model, α is the scaling value between the data and model and σ_{ij}^2 is the data variance. An illustration of this algorithm is shown in Figure 4. Fits were done with both single and binary PSF models, and to assess the statistical significance of the latter we use the one-side F-test.

$$F = \frac{\min(\chi_{single}^2)/\nu_s}{\min(\chi_{binary}^2)/\nu_b} \quad (4)$$

where ν_s and ν_b are the degrees of freedom for the singles and binary fits, respectively, because some parts of the image do not contribute to the fit (i.e. regions with no source flux). So, the degrees of freedom were calculated taking into account the effective pixels involved in the fitting,

$$Pixels_{eff} = \frac{\sum_{ij} M_{ij}}{\max(M_{ij})} \quad (5)$$

$$\nu_{s,b} = Pixels_{eff} - N_{parameters} \quad (6)$$

where $N_{parameters}$ is 3 for the single model, and 6 for the binary (Burgasser et al. 2010).

4.2. Results

The results of these fits are summarized in Table 5 for F127M. The only binary system identified by our PSF-fitting routine was the previously-known wide binary, 2MASS J1520–4422AB with separation $1.20 \pm 0.01''$ and $PA = 29^\circ.65 \pm 0^\circ.70$. These values are marginally consistent with previous determinations (Burgasser et al. 2007). We can conclude that our routine gives us reliable results for resolved BD binary systems.

No other sources were found to be significantly better fit by a binary PSF model, implying that they are single or unresolved with WFC3's resolution and sensitivity.

To check our results is to quantify the relative intensity of the residuals after the primary PSF subtraction. Figure 5 shows the result of this analysis showing images after the PSF subtraction. The 2MASS J1520–4422AB system clearly has the highest residuals compared to the rest of the sample because of its resolved secondary. None of the others targets show clear evidence of multiplicity.

4.3. Searching limits

To assess our detection limits for mid-late T companions we performed a multi-step Monte Carlo simulation

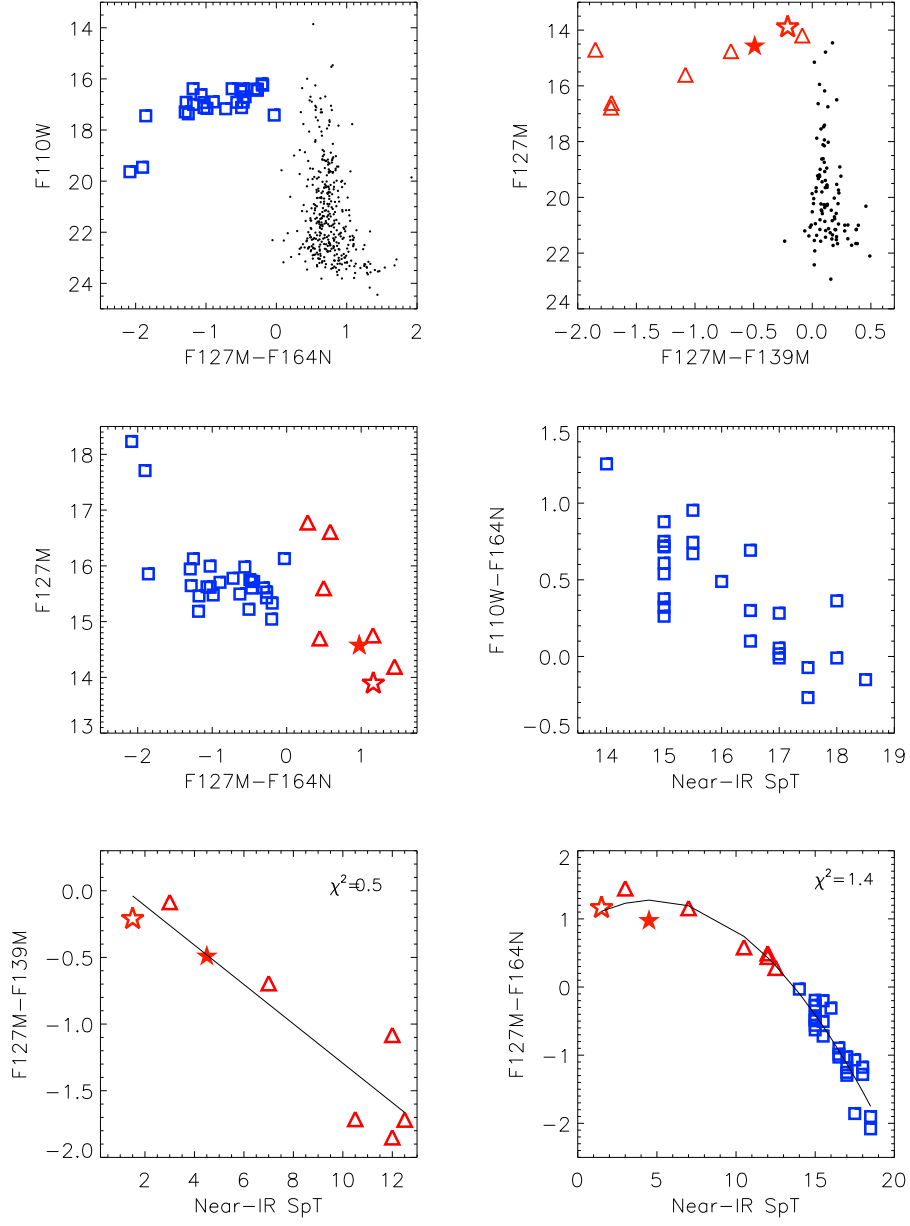


Figure 3. Segregation of L and T dwarfs with WFC3 photometry. Magnitude vs. color and color vs. NIR SpT for 11666 (full blue circles) and 11631 (red triangles) programs, including the known binary system 2MASS J1520-4422AB (red stars), respectively. Background sources are represented by black points. Linear (for F127M-F139M) and quadratic (for F127M-F164N) fits to the photometric data are indicated by the solid lines. Spectral types are encoded as SpT(L0) = 0, SpT(T5) = 15 and, SpT(Y0) = 20. The uncertainties are smaller than the symbol size.

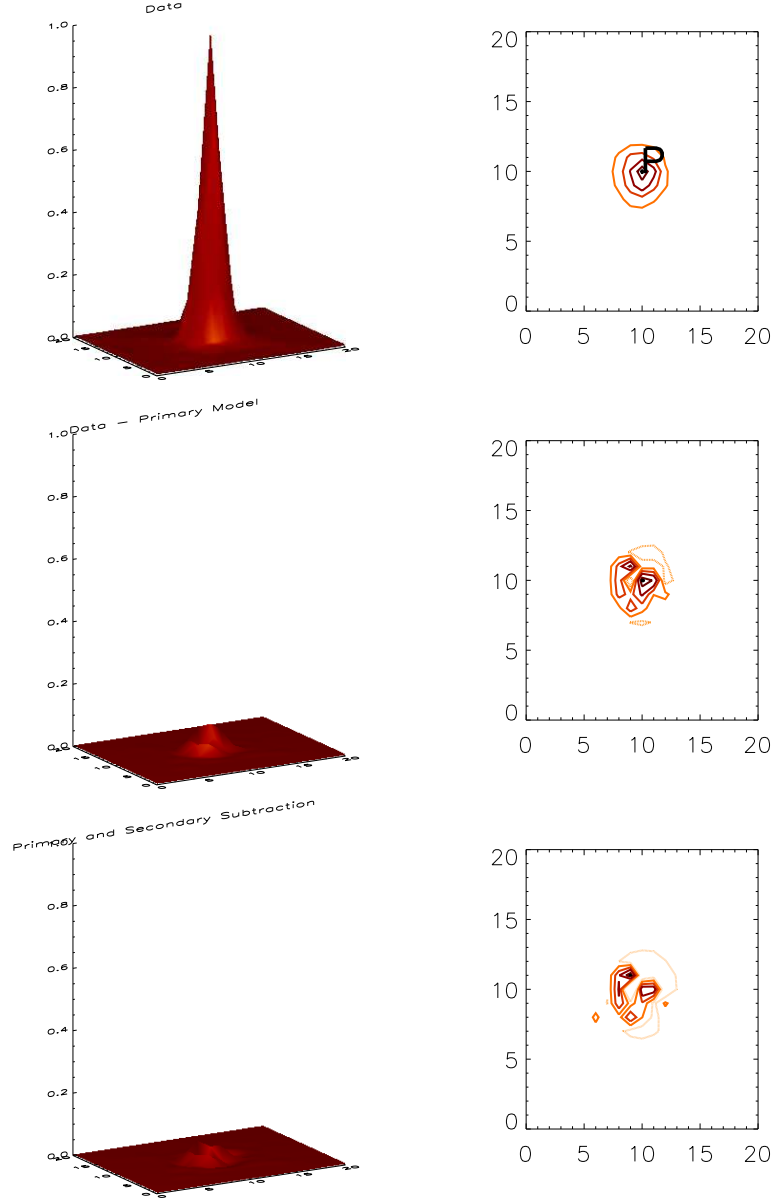


Figure 4. 2MASS J0727+1710 in F127M filter. In the upper part of the figure are shown the surface and contour plots previous to the PSF subtraction. The red letter 'P' represents where the primary BD's coordinates are located. In the middle and bottom part of the figure are shown the surface and contour plots for the residuals after the primary PSF-model subtraction and the residuals after primary and secondary PSF-models subtraction, respectively. The contour levels represent the -0.3 , -0.2 , -0.1 (dashed lines), 0.1 , 0.3 , 0.5 , 0.8 , 0.95 (solid lines) of the maximum flux from the data, and after the primary and secondary PSF-subtraction.

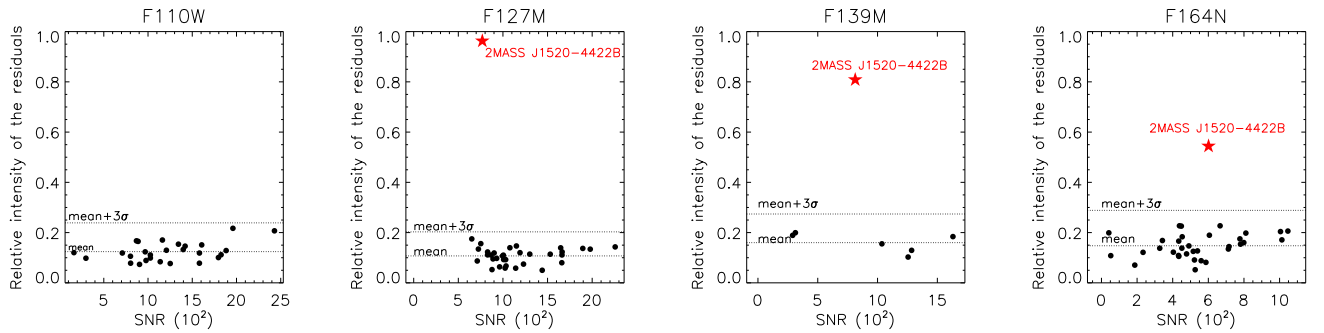


Figure 5. Relative intensity of the residuals after the primary PSF subtraction as a function of the Signal to Noise Ratio. The only object detected is 2MASS J1520-4422B, which is shown with red star above the mean + 3σ value.

Table 5
The statistical Analysis for F127M filter.

Name	χ^2_{single}	χ^2_{binary}	F-test	ρ^a (%)	ρ^a ('')	P.A. ^b °	Δm (mag)
(1)	(2)	(3)	(4)	(5)	(6)	(7)	(8)
Program 11666							
2MASS J0340−6724	95.9	99.4	44	0.83	0.108	69.53	2.82
SDSS J0739+6615	288.7	328.0	40	0.81	0.106	184.96	2.08
2MASS J1013−7842	70.7	52.4	60	1.51	0.197	253.44	2.18
2MASS J1122−3512	5328.8	4908.3	43	0.06	0.008	191.42	2.11
SDSS J1439+3042	100.2	115.7	41	1.19	0.155	118.42	2.14
SDSS J1511+0607	270.7	282.3	43	0.55	0.071	233.01	2.14
2MASS J1520−4422A	0.1	0.01	100	9.23	1.200	29.65	0.04
Program 11666							
ULAS J0034−0052	42.2	42.1	45	0.61	0.080	68.11	2.31
HD 3651B	1878.6	1721.7	44	0.08	0.011	21.14	2.16
2MASS J0050−3322	400.0	369.7	44	0.12	0.015	259.21	2.43
SDSS J0325+0425	686.9	867.8	36	0.88	0.115	115.58	2.27
2MASS J0407+1514	16.3	14.8	50	0.83	0.108	27.53	3.20
2MASS J0510−4208	149.1	162.3	43	0.97	0.126	20.59	2.35
2MASS J0727+1710	173.8	166.0	43	0.0	0.0	304.01	3.08
2MASS J0729−3954	93.3	84.7	48	1.07	0.139	98.61	3.08
2MASS J0741+2351	77.1	62.9	52	1.75	0.227	51.73	2.55
2MASS J0939−2448	68.1	49.5	59	1.84	0.239	122.55	2.39
2MASS J1007−4555	58.7	41.7	60	1.60	0.208	30.35	2.38
2MASS J1114−2618	307.7	302.6	41	0.14	0.018	136.22	2.93
2MASS J1231+0847	513.6	473.0	44	0.09	0.011	69.78	2.30
ULAS J1238+0953	56.5	79.2	33	0.74	0.096	312.23	2.02
SDSS J1250+3925	33.4	34.3	45	0.62	0.080	143.86	2.58
SDSSP J1346−0031	454.4	413.1	44	0.13	0.017	219.76	3.25
SDSS J1504+1027	1100.8	1358.7	37	0.88	0.114	82.03	2.18
SDSS J1628+2308	1139.3	1070.8	43	0.06	0.008	24.22	2.74
2MASS J1754+1649	44.2	53.7	38	1.34	0.174	87.38	2.28
SDSS J1758+4633	571.6	705.5	37	0.88	0.114	122.45	2.36
2MASS J1828−4849	99.6	58.5	68	1.21	0.157	104.86	1.89
2MASS J1901+4718	1203.8	1132.1	42	0.0	0.0	201.57	2.39
SDSS J2124+0100	247.0	234.8	42	0.06	0.008	154.92	2.65
2MASS J21547+5942	472.6	448.1	42	0.12	0.0161	63.44	2.59
2MASS J2237−7228	116.3	108.5	45	1.06	0.138	307.22	2.99
2MASS J2331−4718	106.0	54.5	69	1.59	0.206	44.28	2.39
2MASS J2359−7335	116.2	94.4	53	1.82	0.236	15.22	2.53

^aSeparation between the primary and secondary components after the PSF fitting.

^bPosition angle.

to calculate the detection and false positive rates as a function of separation and relative magnitude for each source in three WFC3 filters (F110W, F127M and F164N). Our simulation used 10^5 fake stars (generated from the PSF model) implanted around each target with different orientations, distances (from 1 to 6 pixels) and Δm (from 0 to 5 mag). Our PSF-fitting routine was then used to recover the implants with steps in distance and magnitude of 0.5 pixels and 0.2 magnitudes to find the limit beyond which the fake stars are not correctly recovered. To quantify the effect of false positives, we performed another Monte Carlo simulation adding 10^3 variations of Gaussian noise to each image and seeing where a (false) secondary is found.

These procedures were done for each source in our sample; an example is shown in Figure 6. Sensitivity maps in Δm and separation were determined based on the fraction of implants recovered, and nulling regions with high false positive rates. We find WFC3 is able to detect companions at separations greater than $0.325''$ and with $\Delta m_{F110W} \leq 2.75$ mag, $\Delta m_{F127M} \leq 3.0$, $\Delta m_{F139M} \leq 2.25$ and $\Delta m_{F164N} \leq 2.5$. Thus, F127M is the most sensitive filter to detect faint companions both due to better image quality (sharper PSF), and since cool (T, Y) companions tend to have a flux distribution that peaks in F127M.

5. ANALYSIS

5.1. Comparison with known mid and late-T dwarfs binary systems

High resolution searches with *HST*/NICMOS-WFPC2 and Keck/NIRC2 instruments have resulted in the detection of seven mid to late T dwarf binary systems at distances closer than 20 pc (see Table 6). With a total of 90 such sources within that distance limit, the corresponding visual BF is $7.8^{+7.5}_{-3.9}\%$. However, a proper comparison requires a quantification of selection effects.

We first calculated the probability of resolving the known mid, late T dwarf binaries in our sample with WFC3. We transformed resolved J magnitudes to F127M using synthetic colors computed from low-resolution near-infrared spectra of L0-T9 dwarfs from the SpeX Prism Spectral Libraries⁵. Figure 7 compares separations and relative magnitudes for these systems to our WFC3 sensitivity limits. Only 2MASS J1553+1532, WISE J0458+6434, WISE J1217+1626 and WISE J1711+3500 are within the WFC3 limits. Multiplying the visual BF with the probabilities $P(\rho \geq 0.325'')$ and $P(\Delta m_{F127M} \leq 3 \text{ mag})$, the probability of finding $T5+ \geq T5$ dwarf binaries in our sample is 4.4%, which is in agreement with the null binary detection in the studied sample.

5.2. Inferring the Binary Fraction of Brown Dwarfs for $T5+$ primary companions.

Given the WFC3 pixel scale, the absence of any new discoveries in this sample is not wholly unexpected. Nevertheless, our sample, is the largest containing $T5+$ sources, so it allows us to more tightly constrain the underlying binary fraction. To do this, we applied the detection and false positive rate maps computed for each source in the F127M filter to another Monte Carlo simulation that determines the probability that each source, if it were a binary, would have been uncovered.

We generated a large sample (5×10^6) of binaries by first drawing primary masses from a power-law mass distribution quantified as $dN/dM \propto M^{-0.5}$ (Burgasser 2004; Burningham et al. 2013). Secondary masses were then computed assuming either a flat mass ratio distribution ($P(q \equiv M_2/M_1) \propto \text{constant}$) or a power-law distribution ($P(q) \propto q^{1.8}$; Allen 2007), imposing a minimum mass of $0.005 M_\odot$. Adopting a uniform age distribution between 0.1 Gyr and 10 Gyr for the simulated systems, the component masses were converted to bolometric luminosities using the evolutionary models of Burrows et al. (2001), and these transformed into spectral types and absolute J magnitudes using the relations given in Dupuy & Liu (2012b). J magnitudes were then transformed to F127M using synthetic colors computed as above. We then computed relative F127M magnitudes for each of the simulated binaries. For the orbits, we assigned semimajor axes assuming either a flat ($P(a) \propto \text{constant}$) or lognor-

⁵ We generated a 6th order polynomial to fit synthetic colors for 543 L0-T9 dwarfs, $F127M-J = \sum_{i=0}^6 a_i \text{SpT}^i$, where $\text{SpT}(L0) = 20$, $\text{SpT}(T0) = 30$, etc. The fit coefficients $\vec{a} = [-9.94976e1, 2.11571e1, -1.84264e0, 8.40307e-2, -2.11748e-3, 2.79814e-5, -1.51800e-7]$ have a standard deviation of 0.016 mag.

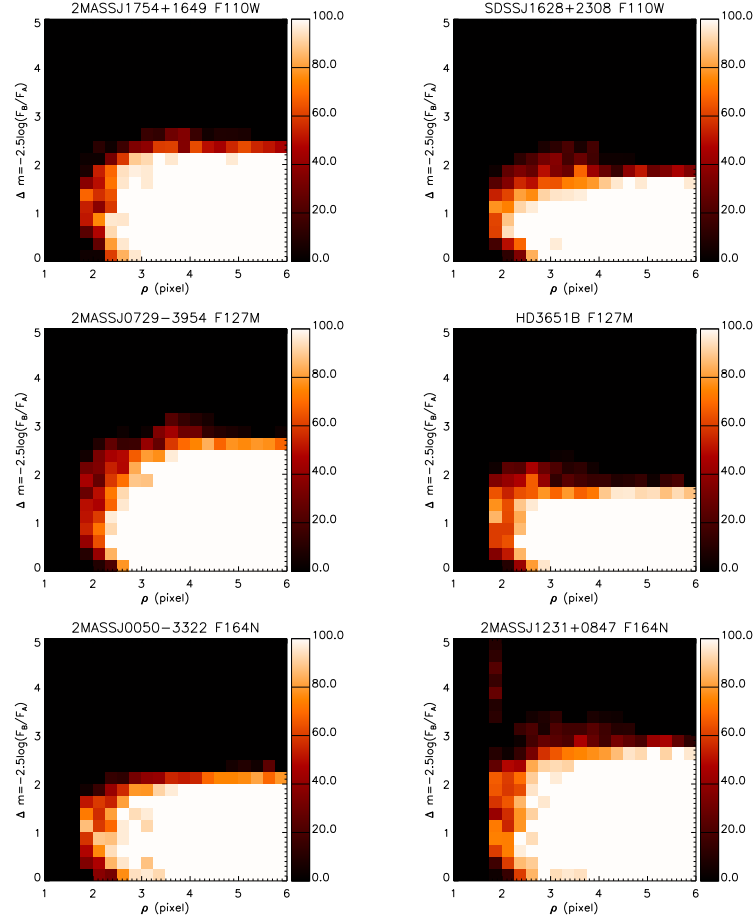


Figure 6. Samples of selection probabilities based on Monte Carlo simulations described in the text, showing 2MASSJ1754+1649 and SDSS J1628+2308 in F110W filter, 2MASS J0729-3954 and HD3651B in F127M filter, and finally 2MASS J0050-3322 and 2MASS J1231+0847 in F164N filter. Detection probabilities are indicated by color scale.

Table 6
Summary of known mid, late-T dwarf binary systems closer than 20 pc.

Object	Instrument	Δm_{F127M} (mag)	ρ (AU)	ρ (mas)	Distance (pc)	Spt. A	Spt. B	Binary Reference
(1)	(2)	(3)	(4)	(5)	(6)	(7)	(8)	(9)
2MASS J1534-2952 ^a	<i>HST</i> WFPC2	0.16 ± 0.28^b	2.3 ± 0.5	140.3 ± 0.57^b	13.6 ± 0.2	T5	T5	Burgasser et al. (2003)
2MASS J1225-2739	<i>HST</i> WFPC2	1.227 ± 0.05	3.8 ± 0.1	282 ± 5	13.4 ± 0.04	T6	T8	Burgasser et al. (2003)
2MASS J1553-1532	<i>HST</i> NICMOS	0.052 ± 0.02	4.2 ± 0.7	349 ± 5	12 ± 2.0	T6.5	T7	Burgasser et al. (2006b)
WISE J0458+6634	Keck NIRC2	0.944 ± 0.09	5 ± 0.4	510 ± 20	10.5 ± 1.4	T8.5	T9	Gelino et al. (2011)
CFBDSIR J1458+1013	Keck NIRC2	1.721 ± 0.07	2.6 ± 0.3	110 ± 5	23.1 ± 2.4	T9.5	>T10	Liu et al. (2011)
WISE J1217+1626	Keck NIRC2	2.021 ± 0.03	8.0 ± 1.3	759.2 ± 3.3	10.5 ± 1.7	T9	Y0	Liu et al. (2012)
WISE J1711+3500	Keck NIRC2	2.722 ± 0.03	15.0 ± 2.0	780.0 ± 2.0	19.0 ± 3.0	T8	T9.5	Liu et al. (2012)

^aThis source was not resolved with WFPC2.

^b Δm and ρ measured by Keck LGS AO observations on K_s filter (Liu et al. 2008).

mal distribution:

$$P(\log a) \propto e^{-\left(\frac{\log a - 0.86}{0.28}\right)^2} \quad (7)$$

(Allen 2007) where a is in AU and constrained to be < 25 AU, a limit which encompasses known T dwarf field binaries. We assumed uniform distributions of mean anomaly, longitude of ascending node, and argument of periaapsis, a $\sin i$ distribution for inclination, and a uniform distribution of eccentricities over $0 < e < 0.6$ based on the analysis of Dupuy & Liu (2011). These orbital elements were projected onto the sky and transformed into angular separations at the distance of each system. We selected only those systems whose primary spectral

type was within 1 subtype of the target, and determined the fraction of these that could have been resolved with WFC3 based on our detection and false positive rate maps. We further assumed that companions wider than $0''.6$ could be detected to the sensitivity limit of each image (Table 2). We computed fractions for the four possible combinations of mass ratio and separation distributions as described above (see Table 7).

Table 7 lists the resulting probabilities of detection, while Figure 8 illustrates how WFC3 selection effects impact observed distributions of binary separation and mass ratio in the case of 2MASS J1828-4849. Not surprisingly, both the closest systems (< 1 AU) and lowest- q

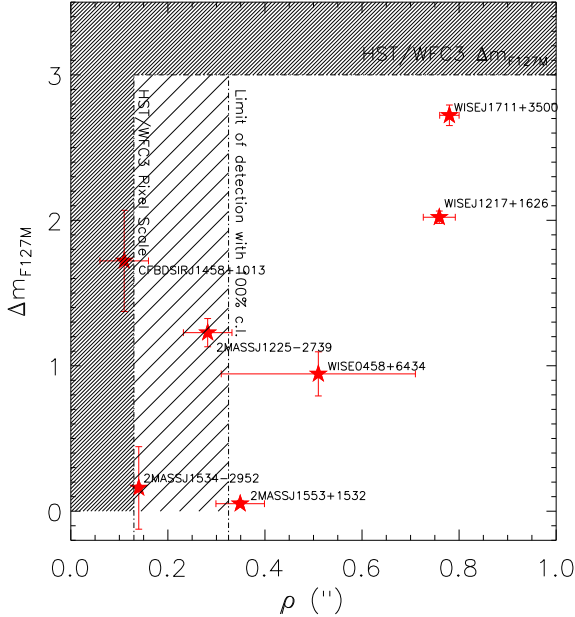


Figure 7. Mid, late-T dwarf binary systems discovered with Keck II LGS-AO and *HST*/NICMOS-WFPC2. Sources are plotted in Δm_{F127M} vs. separation and detection limits for the WFC3 program are overlaid.

systems ($q < 0.6$) are preferentially lost, the latter having the more significant impact on overall recovery rate. The most distant targets in our sample have the lowest detection probabilities and the largest differences in detectability based on the assumed separation distribution, a consequence of the peak of the lognormal distribution falling below angular resolution limits. Detection probabilities are consistently lower for flat versus power-law mass ratio distributions.

By adding up the individual source probabilities, we find that if all our targets had companions we should have detected between 13 and 21 binaries, depending on the assumed underlying distribution. The lack of detections implies a binary fraction upper limit of $<16 - <25\%$ assuming a binomial distribution with 95% of confidence level⁶.

These values are consistent with previous *bias-corrected* estimates of the field brown dwarf binary fraction (Burgasser et al. 2003, 2006b; Allen 2007) and supports the hypothesis that multiplicity rates decline with decreasing primary mass into the substellar regime (see Figure 9; Fischer & Marcy 1992; Reid & Gizis 1997a; Bouy et al. 2003; Close et al. 2003; Kraus & Hillenbrand 2012; Bate 2012). However, our estimates are subject to the same limitations on probing the closely separated (<1 AU) binary population as prior imaging programs. The resolving limit of HST and AO imaging coincides with the peak of the brown dwarf binary separation distribution, suggesting that tighter binaries may be plentiful (Burgasser et al. 2006b). Alternate detection methods such as RV monitoring (e.g., Basri & Martín 1999; Blake et al. 2010) or spectral blend detection (e.g., Burgasser et al. 2010) are still needed to determine if the

⁶ To calculate the confidence limits we use the Clopper-Pearson exact method based on the beta distribution (Brown et al. 2001).

brown dwarf binary fraction may in fact be much higher than imaging studies indicate.

6. CONCLUSIONS

We have analysed data obtained in two imaging survey of 34 BDs with HST/WFC3. The sample comprises 8 L and T dwarfs that we have used to study color-color and color-SpT relations, and 26 mid- to late T dwarfs employed in a search for $\geq T5$ dwarfs companions. Only one previously identified widely-separated system was recovered: 2MASS J1520-4422AB. PSF-fitting uncovered no new close companions to mid-late T sources in our sample.

Based on Monte Carlo simulation we should have been able to detect faint objects at separations $\geq 0.325''$ and with $\Delta m_{F127M} \leq 3.0$. Our failure to detect such companions implies a low binary fraction or a significant population of tight binaries. We determined the fraction of binaries that would have been detected around each source based on assumed separation and mass ratio distributions and all possible orientations of these systems. Due to the WFC3 separation limit that makes the null detection of these sources, we infer an upper limit for the binary fraction of $<16 - <25\%$, depending of the underlying mass ratio distribution. Comparing with previous BD binary surveys made with HST, we can conclude that WFC3 is more sensitive to cool companions than NICMOS and WFPC2 but its lower resolution makes it poorly suited for typically tight brown dwarf binary systems.

Based on observations made with the NASA/ESA Hubble Space Telescope, obtained from the Data Archive at the Space Telescope Science Institute, which is operated by the Association of Universities for Research in Astronomy, Inc., under NASA contract NAS 5-26555. These observations are associated with programs GO-11631 and GO-11666. Support for these programs were provided by NASA through a grant from the Space Telescope Science Institute, which is operated by the Association of Universities for Research in Astronomy, Inc., under NASA contract NAS 5-26555. We acknowledge that this project has benefited from contributions by T. Dupuy, J. Faherty, M. Ireland and M. Liu who were co-investigators and helped develop the original HST proposals, GO 11631 and GO 11666. They provided proprietary information on target selection based on ongoing surveys with ground-based laser guide-star adaptive optics (Liu, Dupuy, and Ireland) and astrometry (J. Faherty). This research has made possible thanks to an international grant from the Spanish Industry Ministry. This research has been supported by the Spanish Virtual Observatory (<http://svo.cab.inta-csic.es>), project funded by MICINN / MINECO through grants AyA2008-02156, AyA2011-24052. This research has benefitted from the M, L, T, and Y dwarf compendium housed at DwarfArchives.org and has benefitted from the SpeX Prism Spectral Libraries, maintained by Adam Burgasser at <http://pono.ucsd.edu/~adam/browndwarfs/spexprism>. Special thanks to Daniella Bardalez Gagliuffi, Juan Carlos Muñoz, Julia Alfonso Garzón and Benjamin Montesinos.

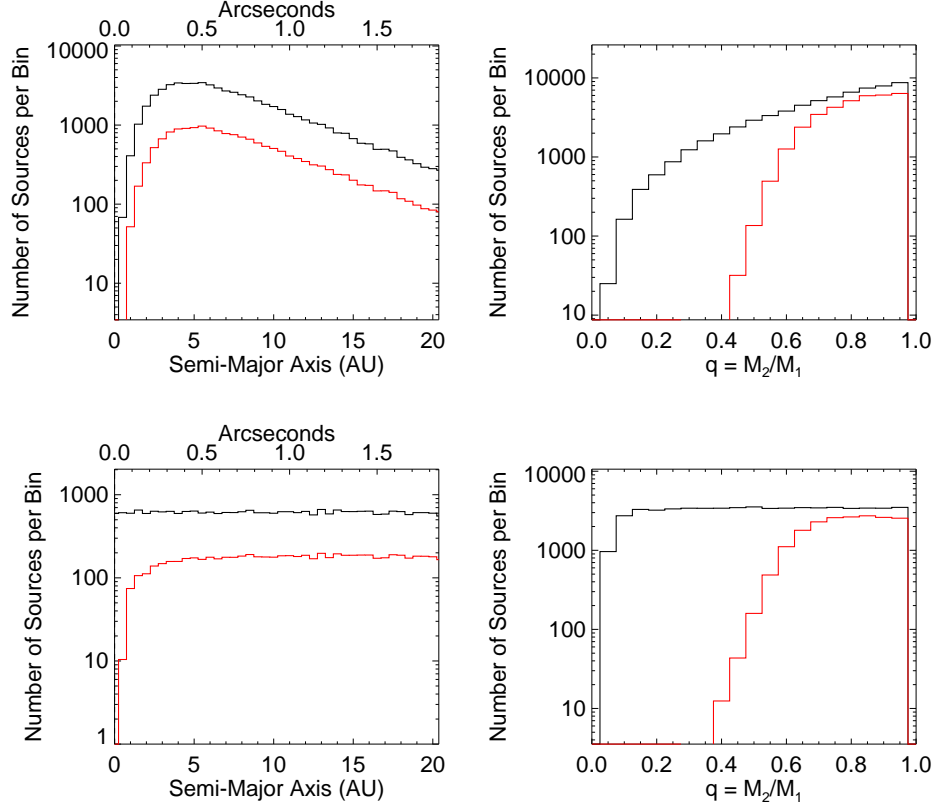


Figure 8. Binary detection probability distributions for the T5.5 2MASS J1828–4849 as a function of semi-major axis (left) and mass ratio (right) based on the simulations described in the text. Each panel displays the distributions of input (black lines) and recovered (red lines) systems based on WFC3 selection function for this source. The top and bottom left panels compare lognormal and constant input distributions for semi-major axis; the top and bottom right panels compare power-law and constant input distributions in mass ratio, respectively. The resulting total binary recovery rate for this and other sources in our sample are given Table 7.

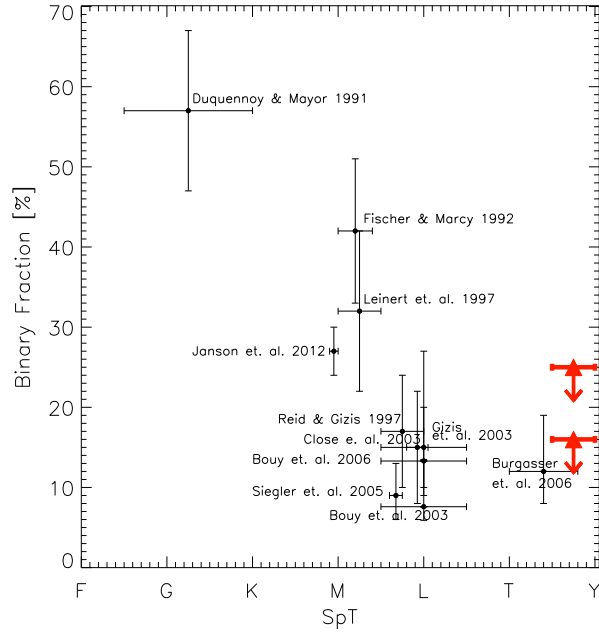


Figure 9. Binary frequency as a function of the spectral type in the field and in clusters. The upper limits determined in this work are shown with red triangles.

Table 7
Companion Detectability with WFC3.

Name	SpT	Distance (pc)	Power-Law q Lognormal a	Power-law q Flat a	Flat q Lognormal a	Flat q Flat a
(1)	(2)	(3)	(4)	(5)	(6)	(7)
ULAS J0034−0052	T8.5	12.6±0.6	82%	84%	60%	61%
HD 3651B	T7.5	11.0±0.1	74%	74%	45%	45%
2MASS J0050−3322	T7.0	8.00±1.0	80%	81%	51%	52%
SDSS J0325+0425	T5.5	19.0±2.0	69%	75%	44%	47%
2MASS J0407+1514	T5.0	17.0±2.0	83%	86%	60%	63%
2MASS J0510−4208	T5.0	18.0±2.0	72%	79%	46%	51%
2MASS J0727+1710	T7.0	9.10±0.2	88%	88%	62%	62%
2MASS J0729−3954	T8.0	6.00±1.0	94%	93%	76%	76%
2MASS J0741+2351	T5.0	18.0±2.0	75%	80%	50%	52%
2MASS J0939−2448	T8.0	10.0±2.0	82%	82%	56%	56%
2MASS J1007−4555	T5.0	15.0±2.0	77%	80%	51%	53%
2MASS J1114−2618	T7.5	10.0±2.0	83%	83%	57%	56%
2MASS J1231+0847	T5.5	12.0±1.0	76%	78%	48%	48%
ULAS J1238+0953	T8.5	18.5±4.3	70%	77%	47%	53%
SDSSP J1346−0031	T6.5	14.5±0.5	82%	87%	59%	63%
SDSS J1504+1027	T7.0	15.9±2.5	69%	75%	42%	46%
SDSS J1628+2308	T7.0	14.0±4.0	78%	82%	52%	56%
2MASS J1754+1649	T5.0	14.3±2.4	74%	77%	46%	48%
SDSS J1758+4633	T6.5	12.0±2.0	76%	77%	48%	48%
2MASS J1828−4849	T5.5	11.0±1.0	69%	73%	40%	43%
2MASS J1901+4718	T5.0	15.0±2.0	75%	80%	48%	52%
SDSS J2124+0100	T5.0	18.0±2.0	74%	79%	50%	52%
2MASS J2154+5942	T5.0	10.0±1.0	86%	86%	60%	61%
2MASS J2237+7228	T6.0	13.0±2.0	79%	82%	51%	55%
2MASS J2331−4718	T5.0	13.0±2.0	78%	81%	50%	52%
2MASS J2359−7335	T6.5	12.3±1.9	79%	80%	51%	52%
Total Expected			20.2	21.0	13.5	14.0
T5+ Dwarf Binary fraction ^a			<17%	<16%	<25%	<23%

^awith 95% of confidence level.

REFERENCES

- Albert, L., Artigau, É., Delorme, P., et al. 2011, *AJ*, 141, 203
- Allen, P. R. 2007, *ApJ*, 668, 492
- Allington-Smith, J., Breare, M., Ellis, R., et al. 1994, *PASP*, 106, 983
- Basri, G., & Martín, E. L. 1999, *AJ*, 118, 2460
- Bate, M. R. 2009, *MNRAS*, 392, 590
- . 2012, *MNRAS*, 419, 3115
- Becklin, E. E., & Zuckerman, B. 1988, *Nature*, 336, 656
- Beichman, C., Gelino, C. R., Kirkpatrick, J. D., et al. 2013, *ApJ*, 764, 101
- Bertin, E., & Arnouts, S. 1996, *A&AS*, 117, 393
- Bihain, G., Scholz, R.-D., Storm, J., & Schnurr, O. 2013, *A&A*, 557, A43
- Bildsten, L., Brown, E. F., Matzner, C. D., & Ushomirsky, G. 1997, *ApJ*, 482, 442
- Blake, C. H., Charbonneau, D., & White, R. J. 2010, *ApJ*, 723, 684
- Bouy, H., Brandner, W., Martín, E. L., et al. 2003, *AJ*, 126, 1526
- Burgasser, A. J. 2004, *ApJS*, 155, 191
- . 2007, *ApJ*, 659, 655
- Burgasser, A. J., Cruz, K. L., Cushing, M., et al. 2010, *ApJ*, 710, 1142
- Burgasser, A. J., Dhital, S., & West, A. A. 2009, *AJ*, 138, 1563
- Burgasser, A. J., Geballe, T. R., Leggett, S. K., Kirkpatrick, J. D., & Golimowski, D. A. 2006a, *ApJ*, 637, 1067
- Burgasser, A. J., Kirkpatrick, J. D., Cruz, K. L., et al. 2006b, *ApJS*, 166, 585
- Burgasser, A. J., Kirkpatrick, J. D., Reid, I. N., et al. 2003, *ApJ*, 586, 512
- Burgasser, A. J.,Looper, D. L., Kirkpatrick, J. D., & Liu, M. C. 2007, *ApJ*, 658, 557
- Burgasser, A. J., McElwain, M. W., Kirkpatrick, J. D., et al. 2004, *AJ*, 127, 2856
- Burgasser, A. J., Kirkpatrick, J. D., Brown, M. E., et al. 2002, *ApJ*, 564, 421
- Burningham, B., et al. 2008, *MNRAS*, 391, 320
- Burningham, B., Cardoso, C. V., Smith, L., et al. 2013, *MNRAS*, 433, 457
- Burrows, A., Hubbard, W. B., Lunine, J. I., & Liebert, J. 2001, *Reviews of Modern Physics*, 73, 719
- Burrows, A., Sudarsky, D., & Lunine, J. I. 2003, *ApJ*, 596, 587
- Chabrier, G., Baraffe, I., Allard, F., & Hauschildt, P. 2000, *ApJ*, 542, L119
- Chiu, K., Fan, X., Leggett, S. K., et al. 2006, *AJ*, 131, 2722
- Choi, J.-Y., Han, C., Udalski, A., et al. 2013, *ApJ*, 768, 129
- Close, L. M., Siegler, N., Freed, M., & Biller, B. 2003, *ApJ*, 587, 407
- Cruz, K. L., Kirkpatrick, J. D., & Burgasser, A. J. 2009, *AJ*, 137, 3345
- Cruz, K. L., Reid, I. N., Kirkpatrick, J. D., et al. 2007, *AJ*, 133, 439
- Cushing, M. C., Kirkpatrick, J. D., Gelino, C. R., et al. 2014, *ArXiv e-prints*, arXiv:1402.1378
- . 2011, *ArXiv e-prints*, *ApJ*, arXiv:1108.4678
- Deacon, N. R., Pinfield, D. J., Lucas, P. W., et al. 2011, in *Astronomical Society of the Pacific Conference Series*, Vol. 448, 16th Cambridge Workshop on Cool Stars, Stellar Systems, and the Sun, ed. C. Johns-Krull, M. K. Browning, & A. A. West, 429
- Delfosse, X., Beuzit, J.-L., Marchal, L., et al. 2004, in *Astronomical Society of the Pacific Conference Series*, Vol. 318, *Spectroscopically and Spatially Resolving the Components of the Close Binary Stars*, ed. R. W. Hilditch, H. Hensberge, & K. Pavlovski, 166–174
- Delorme, P., Willott, C. J., Forveille, T., et al. 2008, *A&A*, 484, 469
- Dupuy, T. J., & Liu, M. C. 2011, *ApJ*, 733, 122
- . 2012a, *ArXiv e-prints*, arXiv:1201.2465
- . 2012b, *ApJS*, 201, 19
- Duquennoy, A., & Mayor, M. 1991, *A&A*, 248, 485
- Epchtein, N., et al. 1997, *The Messenger*, 87, 27
- Faherty, J. K., Burgasser, A. J., Cruz, K. L., et al. 2009, *AJ*, 137, 1
- Faherty, J. K., Burgasser, A. J., Walter, F. M., et al. 2012, *ApJ*, 752, 56
- Fischer, D. A., & Marcy, G. W. 1992, *ApJ*, 396, 178
- Folkes, S. L., Pinfield, D. J., Kendall, T. R., & Jones, H. R. A. 2007, *MNRAS*, 378, 901
- Fruchter, A. S., & Hook, R. N. 2002, *PASP*, 114, 144
- Gelino, C. R., Kirkpatrick, J. D., Cushing, M. C., et al. 2011, *AJ*, 142, 57
- Golimowski, D. A., Nakajima, T., Kulkarni, S. R., & Oppenheimer, B. R. 1995, *ApJ*, 444, L101
- Hamuy, M., Suntzeff, N. B., Heathcote, S. R., et al. 1994, *PASP*, 106, 566
- Hayashi, C., & Nakano, T. 1963, *Progress of Theoretical Physics*, 30, 460
- Kashikawa, N., Aoki, K., Asai, R., et al. 2002, *PASJ*, 54, 819
- Kendall, T. R., Jones, H. R. A., Pinfield, D. J., et al. 2007a, *MNRAS*, 374, 445
- Kendall, T. R., Tamura, M., Tinney, C. G., et al. 2007b, *A&A*, 466, 1059
- Kirkpatrick, J. D., Reid, I. N., Liebert, J., et al. 1999, *ApJ*, 519, 802
- . 2000, *AJ*, 120, 447
- Kirkpatrick, J. D., et al. 2008, *ApJ*, 689, 1295
- Kirkpatrick, J. D., Cushing, M. C., Gelino, C. R., et al. 2011, *ApJS*, in press, arXiv:1108.4677
- Knapp, G. R., Leggett, S. K., Fan, X., et al. 2004, *AJ*, 127, 3553
- Kraus, A. L., & Hillenbrand, L. A. 2012, *ApJ*, 757, 141
- Krist, J. 1995, in *Astronomical Society of the Pacific Conference Series*, Vol. 77, *Astronomical Data Analysis Software and Systems IV*, ed. R. A. Shaw, H. E. Payne, & J. J. E. Hayes, 349–
- Kumar, S. S. 1963, *ApJ*, 137, 1121
- Lawrence, A., et al. 2007, *MNRAS*, 379, 1599
- Liebert, J., Reid, I. N., Burrows, A., et al. 2000, *ApJ*, 533, L155
- Liu, M. C., Dupuy, T. J., Bowler, B. P., Leggett, S. K., & Best, W. M. J. 2012, *ApJ*, 758, 57
- Liu, M. C., Dupuy, T. J., & Ireland, M. J. 2008, *ApJ*, 689, 436
- Liu, M. C., Leggett, S. K., Golimowski, D. A., et al. 2006, *ApJ*, 647, 1393
- Liu, M. C., Delorme, P., Dupuy, T. J., et al. 2011, *ApJ*, 740, 108
- Looper, D. L., Gelino, C. R., Burgasser, A. J., & Kirkpatrick, J. D. 2008, *ApJ*, 685, 1183
- Looper, D. L., Kirkpatrick, J. D., & Burgasser, A. J. 2007, *AJ*, 134, 1162
- Luhman, K. L., Burgasser, A. J., Labbé, I., et al. 2011, *ApJ*, submitted
- Luhman, K. L., Patten, B. M., Marengo, M., et al. 2007, *ApJ*, 654, 570
- Martin, E. L., Basri, G., Delfosse, X., & Forveille, T. 1997, *A&A*, 327, L29
- Martín, E. L., Delfosse, X., Basri, G., et al. 1999, *AJ*, 118, 2466
- Martín, E. L., Phan-Bao, N., Bessell, M., et al. 2010, *A&A*, 517, A53
- Mugrauer, M., Seifahrt, A., Neuhäuser, R., & Mazeh, T. 2006, *MNRAS*, 373, L31
- Mužić, K., Radigan, J., Jayawardhana, R., et al. 2012, *AJ*, 144, 180
- Nakajima, T., Oppenheimer, B. R., Kulkarni, S. R., et al. 1995, *Nature*, 378, 463
- Oppenheimer, B. R., Kulkarni, S. R., Matthews, K., & Nakajima, T. 1995, *Science*, 270, 1478
- Phan-Bao, N., Bessell, M. S., Martín, E. L., et al. 2008, *MNRAS*, 383, 831
- Rebolo, R., Martin, E. L., & Magazzu, A. 1992, *ApJ*, 389, L83
- Rebolo, R., Zapatero-Osorio, M. R., & Martin, E. L. 1995, *Nature*, 377, 129
- Reid, I. N., & Gizis, J. E. 1997a, *AJ*, 113, 2246
- . 1997b, *AJ*, 114, 1992
- Reiners, A., & Basri, G. 2008, *ApJ*, 684, 1390
- Rodler, F., Del Burgo, C., Witte, S., et al. 2011, *A&A*, 532, A31
- Ruiz, M. T., Leggett, S. K., & Allard, F. 1997, *ApJ*, 491, L107+
- Sahlmann, J., Lazorenko, P. F., Ségransan, D., et al. 2013, *A&A*, 556, A133
- Schmidt, S. J., Cruz, K. L., Bongiorno, B. J., Liebert, J., & Reid, I. N. 2007, *AJ*, 133, 2258
- Siegler, N., Close, L. M., Burgasser, A. J., et al. 2007, *AJ*, 133, 2320
- Skrutskie, M. F., et al. 2006, *AJ*, 131, 1163
- Stamatellos, D., & Whitworth, A. P. 2009, *MNRAS*, 392, 413

- Strauss, M. A., et al. 1999, *ApJ*, 522, L61
 Stumpf, M. B., Geißler, K., Bouy, H., et al. 2011, *A&A*, 525, A123
 Tinney, C. G., Burgasser, A. J., & Kirkpatrick, J. D. 2003, *AJ*, 126, 975
 Tinney, C. G., Burgasser, A. J., Kirkpatrick, J. D., & McElwain, M. W. 2005, *AJ*, 130, 2326
 Tinney, C. G., Faherty, J. K., Kirkpatrick, J. D., et al. 2012, *ApJ*, 759, 60
 Tody, D. 1986, in *Society of Photo-Optical Instrumentation Engineers (SPIE) Conference Series*, Vol. 627, Society of Photo-Optical Instrumentation Engineers (SPIE) Conference Series, ed. D. L. Crawford, 733–
 Tsvetanov, Z. I., et al. 2000, *ApJ*, 531, L61
 Vrba, F. J., Henden, A. A., Luginbuhl, C. B., et al. 2004, *AJ*, 127, 2948
 Walkowicz, L. M., Hawley, S. L., & West, A. A. 2004, *PASP*, 116, 1105
 Warren, S. J., et al. 2007, *MNRAS*, 381, 1400
 Wright, E. L., Eisenhardt, P. R. M., Mainzer, A. K., et al. 2010, *AJ*, 140, 1868
 York, D. G., et al. 2000, *AJ*, 120, 1579

APPENDIX

APPENDIX A

2MASSJ1520–4422AB

The only well-resolved target in our sample is the previously identified L dwarf binary 2MASS J1520–4422AB, originally reported by Kendall et al. (2007a) and Burgasser et al. (2007) and found to have an angular separation of 1174 ± 16 mas at position angle $27^\circ 1 \pm 0^\circ 7$ (east of north; epoch 2006 April 8 UT)⁷ and an estimated projected separation of 22 ± 2 AU. Our WFC3 observations yield a separation of $1.20 \pm 0.01''$ and $PA = 29.65^\circ \pm 0.70^\circ$.

The components of this system are classified L1.5 and L4.5 based on NIR spectroscopy, and to date only a combined-light optical spectrum has been reported (Phan-Bao et al. 2008). Because the optical spectra of L dwarfs contain a number of diagnostics of age and mass, including H α emission at 6563 Å and Li I absorption at 6708 Å, we obtained resolved optical spectroscopy of the system using the Low Dispersion Survey Spectrograph (LDSS-3; Allington-Smith et al. 1994) mounted on the Magellan 6.5m Clay Telescope. Observations were obtained on 2006 May 8 (UT) in clear conditions with moderate seeing ($0''.7$ at *R*-band). Data acquisition and reduction procedures are identical to those described in Burgasser et al. (2009).

Figure 10 displays the reduced red optical spectra of both components, compared to equivalent data for the L1 standard 2MASS J14392836+1929149 (Kirkpatrick et al. 1999) and the L4.5 2MASS J22244381–0158521 (Kirkpatrick et al. 2000). The overall spectral morphologies between the 2MASS J1520–4422AB components and templates are in good agreement, confirming the NIR classifications. Note that the 8521 Å Cs I line in 2MASS J1520–4422B is considerably stronger than the template, which may reflect slight differences in temperature, metallicity or surface gravity.

Importantly, neither component shows evidence of H α emission or Li I absorption. The latter implies individual masses greater than $0.065 M_\odot$ (Rebolo et al. 1992; Bildsten et al. 1997) and hence a combined system mass greater than $0.13 M_\odot$. Transforming the measured spectral types into bolometric luminosities using the relation of Burgasser (2007) and comparing these to the evolutionary models of Burrows et al. (2001), we infer a minimum system age of 0.8–1.1 Gyr for 2MASS J1520–4422AB and a minimum primary mass of $0.07 M_\odot$ (Figure 11). This system appears to be a fairly normal, inactive field binary with component masses around the hydrogen burning mass limit.

⁷ In Burgasser et al. (2007), the position angle of this binary is reported as $152.9^\circ 1 \pm 0^\circ 7$, pointing from primary to secondary. However, the authors failed to take into account an image flip in the data, so the actual position angle of the source should have been reported as $27^\circ 1$. Our measurement have been also verified in our LDSS3 acquisition images.

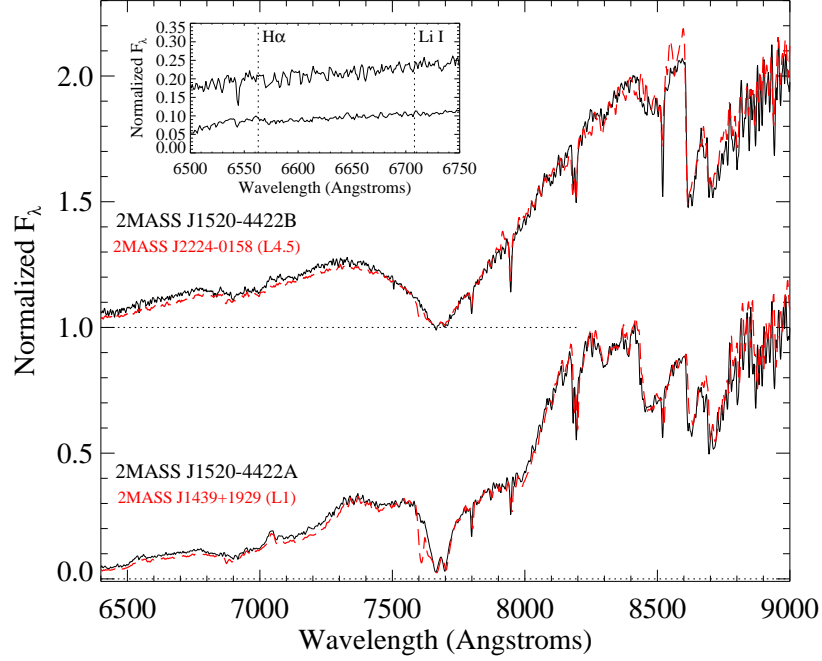


Figure 10. Optical spectra of 2MASS J1520–4422AB (solid black lines) compared to the L1 standard 2MASS J14392836+1929149 (Kirkpatrick et al. 1999) and the L4.5 2MASS J22244381–0158521 (Kirkpatrick et al. 2000; red dashed lines). All spectra are gaussian-smoothed to a common resolution of $\lambda/\Delta\lambda = 1500$ and normalized at 8300 Å, with the L4.5 dwarfs offset by a constant (dotted line). Note that the comparison spectra have not been corrected for telluric absorption (7150–7300 Å; 7600–7650 Å). The inset box highlights the 6500–6750 Å, region revealing no evidence of H α emission or Li I absorption.

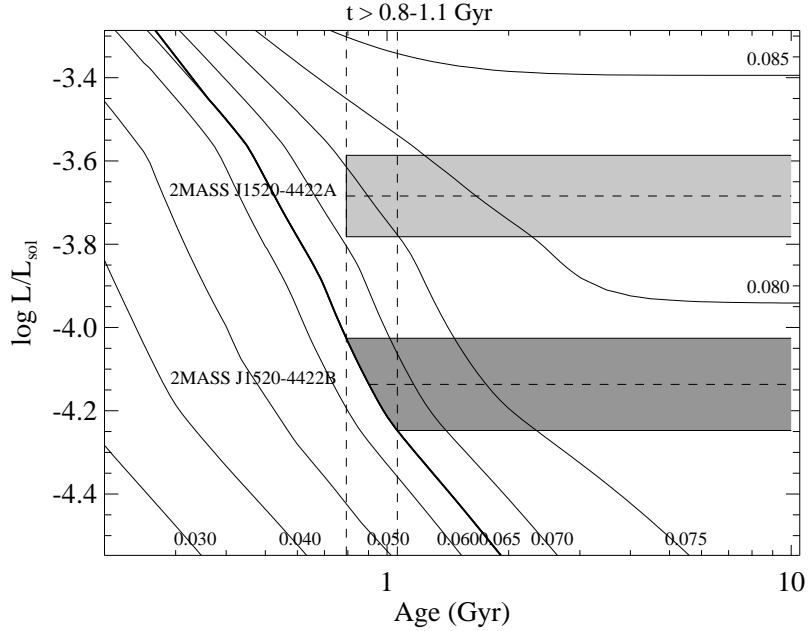


Figure 11. Model-dependent age constraints for the 2MASS J1520–4422AB system, based on the absence of Li I absorption in the component spectra. Bolometric luminosities as a function of time are shown for various masses (labeled in units of M_{\odot}), based on the models of Burrows et al. (2001). Component luminosities of 2MASS J1520–4422AB (horizontal dashed lines) were estimated from the M_{bol}/SpT relation of Burgasser (2007) and include uncertainties in that relation and component optical classifications ($L1 \pm 0.5$ and $L4.5 \pm 0.5$; shaded regions). Assuming a minimum mass of 0.065 M_{\odot} for both components (thick mass track), we infer a minimum system age of 0.8–1.1 Gyr.

APPENDIX B

DENISJ1013–7842

A new source reported here is DENIS J1013–7842, identified in a search for nearby, young, very low-mass objects in the southern sky with DENIS (Looper et al., in prep.). We obtained an optical spectrum of this source with Magellan/LDSS-3 on 2007 May 8 (UT) in clear conditions with $1''.3$ seeing, using the identical configuration as described above but with the slit aligned with the parallactic angle. Two exposures of 1500 s were obtained. The telluric-corrected spectrum is shown in Figure 12 and compared to that of the L3 optical standard 2MASSW J1146345+223053 (Kirkpatrick et al. 1999). The spectra are nearly identical from 6300–9000 Å, with the exception of DENIS J1013–7842 having pronounced $H\alpha$ emission and somewhat weaker TiO absorption at 8500 Å. The $H\alpha$ emission is particularly strong, with an equivalent width (EW) = 10.3 ± 0.2 Å. Using the χ formalism of Walkowicz et al. (2004) with a χ value computed from Reiners & Basri (2008) assuming $T_{eff} = 1950$ K (Vrba et al. 2004), we estimate $\log_{10} L_{H\alpha}/L_{bol} = -5.12 \pm 0.15$ for DENIS J1013–7842, consistent with trends among (rare) active early- and mid-type L dwarfs (Schmidt et al. 2007). The spectrum of this source also shows strong Li I absorption (EW = -5.8 ± 0.2), indicating that it is a brown dwarf with $M < 0.065 M_{\odot}$ and age $\lesssim 750$ Myr (Burrows et al. 2001). There is no evidence of low surface gravity spectral features in this spectrum, however, so this source is likely to be at least 100–300 Myr old (Kirkpatrick et al. 2008; Cruz et al. 2009; Martín et al. 2010).

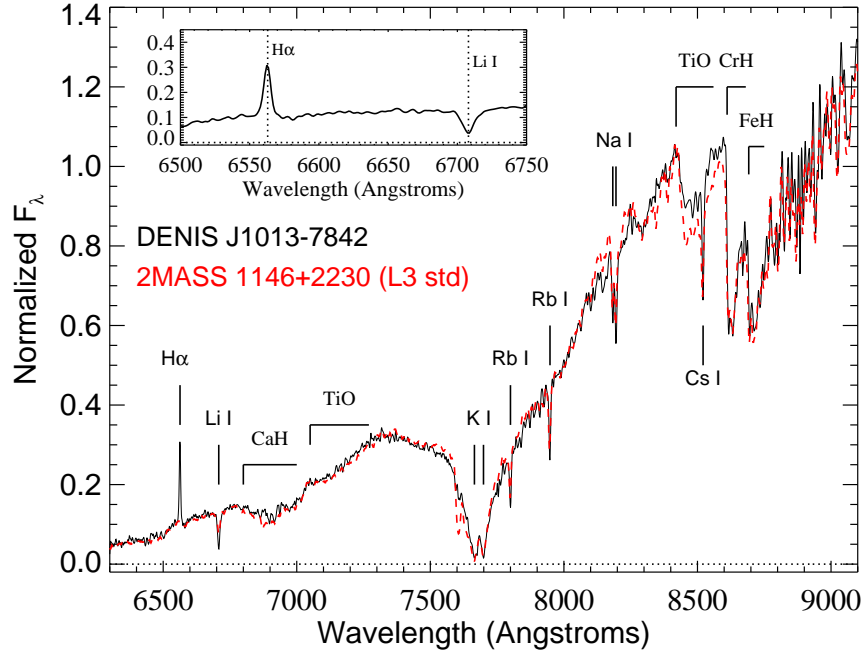


Figure 12. Optical spectrum of DENIS J1013–7842 (solid black line) compared to the L3 standard 2MASSW J1146345+223053 (Kirkpatrick et al. 1999). Both spectra are gaussian-smoothed to a common resolution of $\lambda/\Delta\lambda = 1500$ and normalized at 8400 Å. Note that the comparison spectrum has not been corrected for telluric absorption. The inset box highlights the 6500–6750 Å region showing strong $H\alpha$ emission and Li I absorption.

APPENDIX C

2MASSJ2237+7228

One of our HST targets is the previously unreported T dwarf 2MASS J2237+7228. This source was uncovered by Looper et al. (2007) in a search of the 2MASS survey for mid- and late-type T dwarfs, but at the time of that paper's publication suitable spectral data were unavailable to verify its nature.

Optical spectral data of 2MASS J2237+7228 were obtained with the Subaru 8m Faint Object Camera and Spectrograph (FOCAS) instrument (Kashikawa et al. 2002) on 20 August 2007 (UT) in clear conditions with moderate humidity and light winds. A single 3600 s exposure of the target was obtained with the 0".5 longslit, 150 line/mm grating blazed at 6500 Å and SO58 order-blocking filter, providing 5860–10270 Å spectroscopy at a resolution $\lambda/\Delta\lambda = 400$ and dispersion of 1.3 Å/pixel. A standard flux calibrator from Hamuy et al. (1994) was also observed along with flat field and arc lamps. Data were reduced using the FOCAS reduction pipeline in IRAF⁸; no telluric correction was applied to the data. Figure 13 displays the reduced spectrum compared to equivalent data for the T6 dwarf SDSS J162414.37+002915.6 (Strauss et al. 1999; Liebert et al. 2000), which is an excellent match. We therefore nominally assign an optical classification of T6 for this source.

2MASS J2237+7228 is also detected in the WISE survey ($W2 = 13.62 \pm 0.04$, $W1 - W2 = 2.06 \pm 0.07$), and comparison of 2MASS and WISE coordinates separated by over a decade indicates a modest proper motion: $\mu_\alpha \cos \delta = -73 \pm 2$ mas/yr and $\mu_\delta = -116 \pm 2$ mas/yr. At the estimated 13 ± 2 pc distance⁹ of 2MASSJ2237+7228, this implies a tangential velocity of only 8.3 ± 1.7 km/s, one of the smallest such motions reported for a T dwarf (Faherty et al. 2009).

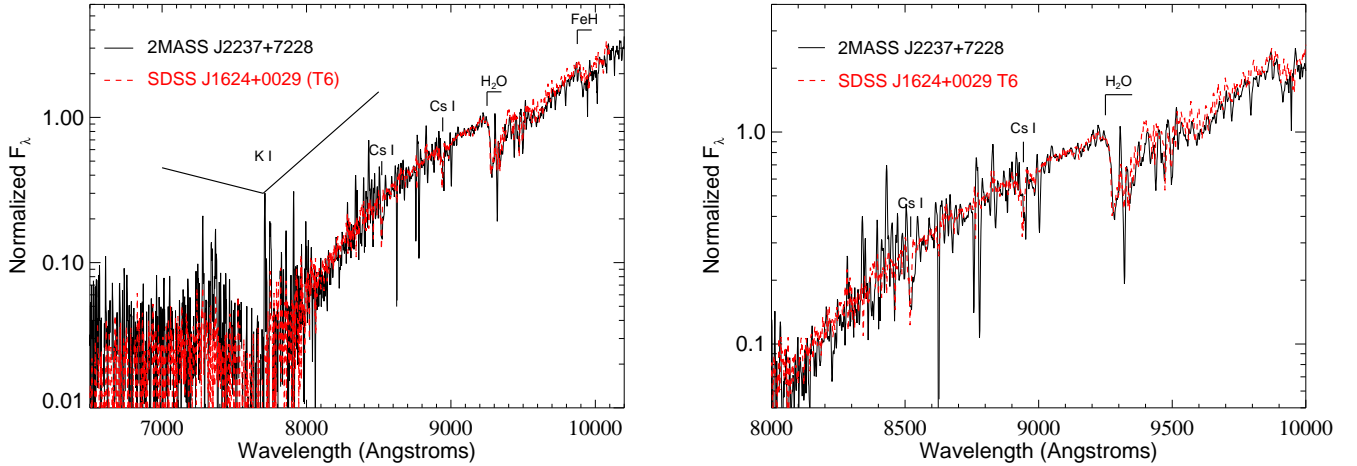


Figure 13. Optical spectrum of 2MASS J2237+7228 obtained with Subaru/FOCAS (black line) compared to equivalent data for the T6 spectral standard SDSS J1624+0029 (red line; data from Liebert et al. 2000). Both spectra are normalized at 9500 Å and plotted on a logarithmic vertical scale. Primary absorption features in the red optical spectra of T dwarfs are indicated.

⁸ Image Reduction and Analysis Facility; Tody (1986).

⁹ This estimate is based on the 2MASS *J*-band magnitude of the source ($J = 15.76 \pm 0.07$) and the absolute-magnitude/spectral type relation from Looper et al. (2008), assuming an ± 0.5 uncertainty on the subtype.